Vortex crystals on the surface of a torus

Takashi Sakajo *

Abstract

Vortex crystals on the surface of a torus are relative equilibrium states of point vortices rotating at a constant speed in the latitudinal direction without changing their relative configurations. They are examples of stationary lattice structures subject to the logarithmic particle interaction energy, which give rise to phenomenological models applicable to incompressible fluids, superconductors, superfluids and Bose-Einstein condensates. The problem of finding vortex crystals is formulated as a linear algebraic null equation $A\mathbf{\Gamma} = 0$ for a non-normal matrix A whose entities are obtained by the locations of point vortices, and $\mathbf{\Gamma}$ consisting of the strengths of point vortices and the latitudinal speed of rotation. Vortex crystals are obtained numerically by prescribing their locations and/or by moving them randomly so that the matrix A becomes rank-deficient through the singular value decomposition. Their strengths are taken from the null-space corresponding to the zero singular values. We find many vortex crystals that are specific to the toroidal geometry: the existence of a handle structure. (i) Polygonal arrangement of point vortices around the handle; (ii) multiple latitudinal polygonal ring configurations of point vortices that are evenly arranged around the handle; (iii) point configurations arranged along helical curves associated with the fundamental group of the toroidal surface. We observe the strength of point vortices and the behavior of their distribution as the number of point vortices gets larger. We also investigate their linear stability and randomness as point configurations.

1 Introduction

For a 2D velocity field $(u_1(x,y), u_2(x,y))$ at $(x,y) \in \mathbb{R}^2$, the vorticity is defined by a scalar function, i.e., $\omega = \partial_y u_1 - \partial_x u_2$ This is an important quantity describing the evolution of incompressible 2D fluid flows, since interactions between high vorticity regions give rise to various complicated flow dynamics. When the fluid flow subject to an external forcing is confined in 2D planar domains, those high vorticity regions are localized and self-organizing into a beautiful stationary lattice structure owing to their mutual interactions. For instance, in an experiment of small magnetic discs at a thin liquid-air interface under the influence of a magnetic field, ring lattice structures of the discs at the centers of vorticity regions are formed owing to a balance between the magnetic attractive interaction among the discs and a hydrodynamic repulsive interaction associated with spinning fluid motion [19]. Another experiment of magnetized electrons in a 2D turbulent flow shows that, in the relaxation process of the turbulence, the merger of vortex structures leads to the formation of regular lattice patterns of vortices [18], whose physical process has been investigated by numerical simulations [20].

Lattice structures of vorticity regions are observed not only in fluid flows, but also in the other physical phenomena such as superconductors, superfluid helium and Bose-Einstein condensates. Abrikosov [2] predicted the existence of a 2D lattice structure of magnetic flux lines in type II superconductors, which is experimentally confirmed by Essmann and Träuble [16]. This is a counterpart of localized vorticity regions in electromagnetic fields. On the other hand, after Feynman's publication on the formation of vortex tubes in superfluid helium [17], the existence of stable ring lattices of vortex lines with quantized circulations was confirmed in an experiment of rotating superfluid film [38]. Recently, with a development of experimental techniques, the formation of various vortex lattice structures, not limited to regular lattices and ring structures, has been observed in many experiments of Bose-Einstein condensates. We can find those pattern in Abo-Shaeer et al. [1] and Engels et al. [14, 15].

*Department of Mathematics, Kyoto University, Kitashirakawa Oiwake-cho, Kyoto 606-8502, JAPAN, E-mail: sakajo@math.kyoto-u.ac.jp

The discoveries of such vortex lattices consisting of many vortex structures motivate us to develop a mathematical model based on the interactions among vortex structures, which we call *"Vortex lattice theory"*. The model is based on the assumption that the azimuthal velocity field induced by the localized vortex structure depends only on the radius r, and it decays as $1/r$ as r goes infinity. A good survey of the model's history and the related references was given by Newton and Chamoun [27], in which we also found a discussion in the Nobel Lecture by Aborisokov [3] for its physical relevance. This model is phenomenological and different from solving partial differential equations such as the Navier-Stokes equations and the Ginzburg-Landau/Gross-Pitaevskii equations with localized vorticity initial data, but it is flexibly extendable to problems finding many vortex lattices when the number of vortex structures is large and when we consider vortex structures on domains with various geometric properties such as 2D curved surfaces and 2D domains with many boundaries.

Toward theoretical understanding of the lattice formation of localized vortex structures, assuming that the high vorticity regions concentrate in a finite set of isolated points, we then express the vorticity as a Dirac's delta measure whose support consists of those points, which are called *point vortices*. Under this assumption, the interaction of localized vorticity regions simply depends on their inter-particle distance and decays as $1/r$ for large r as desired. However, the vorticity is no longer a meaningful quantity since it diverges at the points, while the circulation, i.e., $\int_C \boldsymbol{u} \cdot ds$ for a closed Jordan curve C around the point, still effectively represents the strength of the point vortex. The lattice structure of point vortex, in which their relative configuration remains unchanged throughout the evolution, is called a *vortex crystal* which we shall consider here.

The study of vortex crystals in planar domains has a long history, dating back to the "vortex atom" theory of matter by Thomson [36] in 1860s. It is reformulated in a modern framework by Campbell and Ziff [9], where a catalogue of vortex crystals in a circular disc domain was provided. Aref et al. [5] and Newton [26] survey the mathematical aspects of vortex crystals and gave many vortex crystals in planar domains with/without boundaries, on a sphere and the hyperbolic plane. Fixed vortex equilibria in multiply connected domains with boundaries are constructed [31]. More vortex crystals on the sphere and their stability have been intensively studied, since they have geophysical relevances [8, 23, 24, 29, 30].

In the present paper, we study vortex crystals on the surface of a torus. The toroidal surface has different geometric properties from the 2D plane and the spherical surface: it has non-constant curvature and a non-trivial handle structure. Importance of vortices in curved surfaces is discussed by Turner et al. [37]. 0n the other hand, the vortex crystal on the toroidal surface is supposed to be a particle-interaction based model of quantized vortex lattice in superfluid helium on the surface of a porous medium [10, 25] as in the planar case. There is another application of vortex crystals to find good point configurations on the toroidal surface, since mesh generation on curved surfaces based on the physical particle interaction is utilized in computer graphics community [11, 39]. Only a few number of vortex crystals on the toroidal surface are known so far. Sakajo and Shimizu [33] have shown the existence of three kinds of vortex crystals; (i) Point vortices located at antipodal points; (ii) the polygonal ring configuration of N identical point vortices along the line of latitude; and (iii) a symmetric two latitudinal ring configurations of point vortices with the strengths of the opposite signs. The purpose of this paper is providing more vortex crystals and discuss their properties such as linear stability and randomness as point configurations.

There are two ways to obtain vortex crystals. The first one is an "ansatz-based" approach, where one prescribes the locations and the strengths of point vortices by assuming certain discrete symmetries and confirm whether or not they form vortex crystals. Owing to the construction, most of the vortex crystals obtained by the ansatz-based approach become symmetric. On the other hand, asymmetric vortex equilibrium states in the unbounded plane have also been constructed by solving a nonlinear equation [4]. The second approach is a stochastic numerical method called *the Brownian ratchet scheme*, where point configurations of vortex crystals are searched by moving points randomly. This method was proposed by Newton and Chamoun [28] based on a linear algebraic formulation. It was successfully applied to produce many symmetric and asymmetric point vortex equilibria in the unbounded plane [28] and on the spherical surface [29, 30].

This paper is organized as follows. In Section 2, we provide a linear algebraic formulation of finding vortex crystals on the surface of a torus based on the evolution equations of N point vortices given by Sakajo and Shimizu [32]. Using an ansatz-based approach, we construct ring configurations of vortex crystals that acquire certain longitudinal and latitudinal discrete symmetries and their properties when the number of

point vortices gets larger in Section 3. We also discuss their linear stability and some stochastic properties as point configurations on the surface. The Brownian ratchet scheme is utilized to provide another family of vortex crystals that are arranged going along a line of helical curve around the handle of the torus in Section 4. The final section is devoted to concluding remarks.

2 Formulation of vortex crystals on a toroidal surface

Let $\mathbb{T}_{R,r}$ denote the toroidal surface of major radius R and minor radius r. Its modulus is the aspect ratio $\alpha = R/r > 1$, by which we define the two parameters $\mathcal{A} = (\alpha^2 - 1)^{-1/2}$ and $\rho = \exp(-2\pi\mathcal{A})$. Suppose that the locations of N point vortices on the toroidal surface at time t are given by $(\theta_m(t), \phi_m(t)) \in \mathbb{R}/2\pi\mathbb{Z} \times \mathbb{R}/2\pi\mathbb{Z}$ and $\Gamma_m \in \mathbb{R}$ are their strengths, which are circulations around the point vortices, for $m = 1, \ldots, N$. In 3D Euclidean space, their locations are represented by

$$\iota\colon (\theta_m, \phi_m) \in \mathbb{T}_{R,r} \mapsto ((R - r\cos\theta_m)\cos\phi_m, (R - r\cos\theta_m)\sin\phi_m, r\sin\theta_m) \in \mathbb{E}^3.$$

We introduce a complex coordinate in the annular domain $\mathcal{D} = \{\zeta \in \mathbb{C} \,|\, \rho < |\zeta| < 1\}$ associated with the toroidal surface through the following stereographic projection.

$$\zeta\colon (\theta_m, \phi_m) \in \mathbb{T}_{R,r} \mapsto \mathrm{e}^{\mathrm{i}\phi_m} \exp\left(- \int_0^{\theta_m} \frac{\mathrm{d}u}{\alpha - \cos u} \right) \equiv \mathrm{e}^{\mathrm{i}\phi_m} \exp(r_c(\theta_m)) \in \mathcal{D}, \tag{1}$$

in which $r_c(\theta)$ is defined by

$$r_c(\theta) = - \int_0^{\theta} \frac{\mathrm{d}u}{\alpha - \cos u} = \ |\zeta|.$$

Let $P(\zeta)$ denote the Schottky-Klein prime function associated with the annular domain $\mathcal{D}$,

$$P(\zeta) = (1 - \zeta) \prod_{n \geqq 1} (1 - \rho^n \zeta)(1 - \rho^n \zeta^{-1}).$$

The evolution equation of N point vortices located at $(\theta_m(t), \varphi_m(t))$ has been described as follows [32].

$$\dot{\theta}_m = \sum_{j \neq m}^{N} \Gamma_j F_{mj} := F_m(\theta_1, \ldots, \theta_N, \varphi_1, \ldots, \varphi_N), \tag{2}$$

$$\dot{\varphi}_m = \sum_{j \neq m}^{N} \Gamma_j G_{mj} + \Gamma_m H_m := G_m(\theta_1, \ldots, \theta_N, \varphi_1, \ldots, \varphi_N), \tag{3}$$

in which $\cdot$ denotes the temporal derivative, and F_{mj}, G_{mj} and H_m are specified by

$$F_{mj} = \frac{\mathrm{i}}{r^2(\alpha - \cos\theta_m)} \left[\frac{K(\zeta_m/\zeta_j) - \overline{K(\zeta_m/\zeta_j)}}{4\pi} \right], \tag{4}$$

$$G_{mj} = \frac{1}{r^2(\alpha - \cos\theta_m)^2} \left[\frac{K(\zeta_m/\zeta_j) + \overline{K(\zeta_m/\zeta_j)}}{4\pi\alpha} + \frac{\alpha\theta_m - \sin\theta_m}{4\pi^2\alpha} + \frac{r_c(\theta_j)}{4\pi\mathcal{A}} - \frac{1}{4\pi} \right], \tag{5}$$

$$H_m = \frac{1}{r^2(\alpha - \cos\theta_m)^2} \left[\frac{\alpha\theta_m - \sin\theta_m}{4\pi\alpha^2} + \frac{r_c(\theta_m)}{4\pi^2\mathcal{A}} + \frac{1}{4\pi}\sin\theta_m \right]. \tag{6}$$

Here, $\zeta_m = \zeta(\theta_m, \phi_m)$ is the complex representation (1) of the mth point vortex and the function $K(\zeta)$ is defined by $K(\zeta) = \zeta P_\zeta(\zeta)/P(\zeta)$. Suppose that N point vorties form a vortex crystal, which is a relative equilibrium state rotating at a constant speed V_0 in the latitudinal direction, say, $\theta_m(t) = \vartheta_m$ and $\phi_m(t) = \varphi_m + V_0 t$. Substituting the ansatz into the equations (2) and (3), we obtain the following

algebraic equations for the vortex crystal.

$$\sum_{j\neq m}^{N} \Gamma_j F_{mj}(\vartheta_1,\ldots,\vartheta_N,\varphi_1,\ldots,\varphi_N) = 0, \tag{7}$$

$$\sum_{j\neq m}^{N} \Gamma_j G_{mj}(\vartheta_1,\ldots,\vartheta_N,\varphi_1,\ldots,\varphi_N) + \Gamma_m H_m(\vartheta_1,\ldots,\vartheta_N) - V_0 = 0. \tag{8}$$

Note that the equations (2) and (3) are reformulated as a Hamiltonian dynamical system with its Hamiltonian function $\mathcal{H}$ given by

$$\mathcal{H}(\theta_1,\ldots,\theta_N,\phi_1,\ldots,\phi_N) = -\frac{1}{2}\sum_{m=1}^{N}\sum_{j\neq m}^{N} \Gamma_m\Gamma_j G_H(\zeta_m,\zeta_j) - \frac{1}{2}\sum_{m=1}^{N}\Gamma_m^2 R(\zeta_m), \tag{9}$$

where

$$G_H(\zeta_m,\zeta_j) = \frac{1}{2\pi}\log|\zeta_j P(\zeta_m/\zeta_j)| + \frac{1}{4\pi^2\mathcal{A}} r_c(\theta_m) r_c(\theta_j) + F(\theta_m) + F(\theta_j) + \frac{1}{4\pi} r_c(\theta_m) + \frac{1}{4\pi} r_c(\theta_j), \tag{10}$$

$$R(\theta_m) = \frac{1}{2\pi}\log\prod_{n\geq 1}(1-\rho^n)^2 + \frac{1}{4\pi^2\mathcal{A}} r_c^2(\theta_m) + 2F(\theta_m) + \frac{1}{2\pi} r_c(\theta_m) - \frac{1}{2\pi}\log(R - r\cos\theta_m) \tag{11}$$

and the auxiliary indefinite integral $F(\theta)$ is defined by

$$F(\theta) = -\frac{1}{4\pi^2\alpha}\int_0^\theta \frac{\alpha u - \sin u}{\alpha - \cos u}\mathrm{d}u.$$

Hence, any vortex crystal is a critical point of the Hamiltonian function (9) containing the logarithmic particle interaction energy term.

We here regard the equations (7) and (8) as a linear (null) equation $A\boldsymbol{\Gamma} = \mathbf{0}$, in which the $(2N+1)\times(N+1)$ real matrix A are computed from the locations (ϑ_m,φ_m) of N point vortices and a vector $\boldsymbol{\Gamma}\in\mathbb{R}^{N+1}$ is given by

$$A = \begin{bmatrix} 0 & F_{12} & \cdots & F_{1N} & 0 \\ F_{21} & 0 & \cdots & F_{2N} & 0 \\ \vdots & \vdots & \ddots & \vdots & \vdots \\ F_{N1} & F_{N2} & \cdots & 0 & 0 \\ H_1 & G_{12} & \cdots & G_{N1} & -1 \\ G_{21} & H_2 & \cdots & G_{2N} & -1 \\ \vdots & \vdots & \ddots & \vdots & \vdots \\ G_{N1} & G_{N2} & \cdots & H_N & -1 \end{bmatrix}, \qquad \boldsymbol{\Gamma} = \begin{bmatrix} \Gamma_1 \\ \Gamma_2 \\ \vdots \\ \Gamma_N \\ V_0 \end{bmatrix}.$$

The matrix A is called the *configuration matrix*, since it encodes the geometric information on the configuration of the point vortices on the toroidal surface. The solution vector $\boldsymbol{\Gamma}$ is referred to as *an extended strength vector*, since it consists of the strengths of N point vortices and the latitudinal speed of rotation V_0. When we find a point configuration satisfying $\det(A^TA) = 0$, the configuration matrix A becomes rank deficient and has a non-trivial null space. Hence, if $\mathrm{Rank}(A) = k$, then the extended vortex strength vector $\boldsymbol{\Gamma}$ belongs to $N+1-k$ dimensional null space. In particular, when the rank of the null space to the configuration matrix A is one, which is the case for the most of vortex crystals obtained in this paper, we identify the strength Γ_m of the mth point vortex uniquely up to $\pm$ sign under a certain normalization condition. The null space of A is easily constructed by the singular value decomposition. Let $\sigma_m\in\mathbb{R}$, $\boldsymbol{u}_m\in\mathbb{R}^{2N+1}$ and $\boldsymbol{v}_m\in\mathbb{R}^{N+1}$, $m=1,\ldots,N+1$ denote the singular values and their corresponding left and right singular vectors, which are obtained by solving the coupled linear systems $A\boldsymbol{v}_m = \sigma_m\boldsymbol{u}_m$ and $A^T\boldsymbol{u}_m = \sigma_i\boldsymbol{v}_m$ with $\sigma_1 \geqq \sigma_2 \geqq \cdots \geqq \sigma_{N+1} \geqq 0$.

As discussed by Newton and Chamoun [27], the singular values of the configuration matrix A for a given vortex crystal measure how disorderly the point vortices are distributed on the surface of a torus. Suppose

that we define the normalized eigenvalues by $\widehat{\lambda}_m = \lambda_m / \sum_{n=1}^{k} \lambda_n$ for $m = 1, \ldots, k$ with $k = \mathrm{Rank}(A)$, where $\lambda_m = (\sigma_m)^2$ is the eigenvalues to the covariance matrix $A^T A$. Then the sequence $(\widehat{\lambda}_1, \cdots, \widehat{\lambda}_k)$ is regarded as a discrete stochastic distribution, for which we introduce the *entropy* as follows.

$$S = -\sum_{m=1}^{k} \widehat{\lambda}_m \ln \widehat{\lambda}_m.$$

If the configuration matrix is a random matrix, its corresponding entropy takes the maximum $S_{\max} = \ln N$, since the stochastic distribution is uniform, i.e., $\widehat{\lambda}_m = 1/N$ for all $m \leqq k$. On the other hand, the minimum entropy $S_{\min} = 0$ is attained for the most ordered state $\widehat{\lambda}_1 = 1$ and $\widehat{\lambda}_k = 0$ for $k \geqq 2$. Accordingly, the entropy ratio $\omega_N = S/\ln N$ $(0 < \omega_N < 1)$ becomes a measure of "disorder" of the point configuration for a vortex crystal. In addition, Newton and Chamoun [27] also discussed that vortex crystals with high entropy ratio ω_N become more "robust" than those with low entropy ratio, since the entropy tends to increase when a point configuration is subject to generic perturbations,

Once the point configuration of a vortex crystal and its corresponding normalized strengths are specified, we easily check its linear stability by computing the eigenvalues to the Jacobi matrix $\mathcal{L} \in \mathbb{R}^{2N \times 2N}$ of (2) and (3) linearized around the configurations. Each component of $\mathcal{L}$ is approximated numerically by the standard forward finite difference. For instance, its (m, j) component L_{mj} for $m, j = 1, \ldots, N$ is computed by

$$L_{mj} = \frac{\partial F_m}{\partial \theta_j} \approx \frac{1}{h}[F_m(\vartheta_1, \ldots, \vartheta_j + h, \ldots, \vartheta_N, \varphi_1, \ldots, \varphi_N) - F_m(\vartheta_1, \ldots, \vartheta_j, \ldots, \vartheta_N, \varphi_1, \ldots, \varphi_N)]$$

for a sufficiently small $h > 0$. Since the equations (2) and (3) are written as a Hamiltonian dynamical system, the eigenvalues of the Jacobi matrix $\mathcal{L}$ become either a pair of real numbers with the opposite signs or a conjugate pair of pure imaginary numbers. Let $\{\mu_m\}_{m=1}^{2N}$ denote the eigenvalues to the linearized matrix $\mathcal{L}$, and $\mu_{\mathcal{L}}^N$ be the maximum of the real part of the eigenvalues, i.e., $\mu_{\mathcal{L}}^N = \max_{1 \leqq m \leqq 2N} \mathrm{Re}(\mu_m)$. Then, the vortex crystal is linearly unstable when $\mu_{\mathcal{L}}^N > 0$, while it is neutrally stable when $\mu_{\mathcal{L}}^N = 0$.

3 Ring configurations

A latitudinal polygonal ring configuration of identical N point vortices is called *an N-ring*, whose locations are given by

$$\vartheta_m = \Theta_0, \qquad \varphi_m = \frac{2\pi}{N} m, \qquad \Gamma_m = \Gamma, \qquad m = 1, \ldots, N, \tag{12}$$

for $\Theta_0 \in \mathbb{R}/2\pi\mathbb{Z}$ and $\Gamma \in \mathbb{R}$. It is shown that this configuration becomes a vortex crystal [32] and its linear stability and nonlinear evolutions have been investigated by Sakajo and Shimizu [33]. In this section, we consider the other two families of ring configurations of N point vortices that acquire a discrete rotational symmetry in the longitudinal direction and confirm if they are vortex crystals.

3.1 Longitudinal vortex rings

Suppose that N point vortices are polygonally arranged along the line of longitude $\phi = 0$. Owing to the discrete longitudinal rotational symmetry by the angle $\gamma_0 = 2\pi/N$, their locations are specified by

$$\vartheta_m = \frac{2\pi}{N}(m-1) + \gamma, \qquad \varphi_m = 0, \qquad m = 1, \ldots, N, \tag{13}$$

for $\gamma \in [0, \gamma_0)$. We here refer the configuration (13) to as *a longitudinal N-ring*. Figure 1 is an illustration of a longitudinal 6-ring on the toroidal surface of $R = 3$ and $r = 1$, i.e., $\alpha = 3.0$, in 3D Euclidean space. The first point vortex with the strength Γ_1 is set at $\vartheta_1 = \gamma$ and $\varphi_1 = 0$ and the others are polygonally arranged around the line of longitude $\phi = 0$ in the counter-clockwise direction.

The longitudinal 2-ring is always a vortex crystal. In particular, for $\gamma = 0$, the dimension of the null-space of the configuration matrix A is four, since it corresponds to an antipodal configuration that has

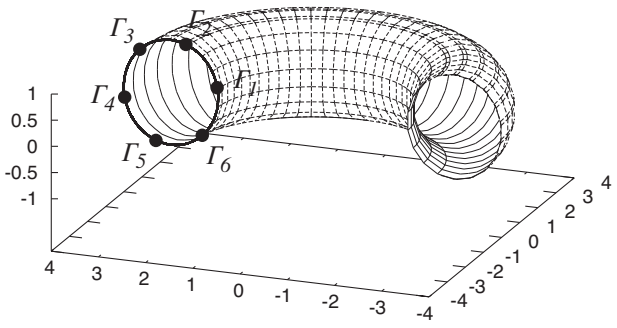

Figure 1: A longitudinal 6-ring configuration. The configuration of point vortices forms a regular hexagon arranged along the line of longitude $\phi = 0$ of the toroidal surface $\mathbb{T}_{R,r}$ of aspect ratio $\alpha = R/r$ with $R = 3$ and $r = 1$. For the sake of visibility, we cut the torus in half and show its section to show the configuration clearly.

an additional symmetry. Even when $\gamma \neq 0$, it still gives a vortex crystal, but its corresponding null-space is one-dimensional and their strengths become the same magnitude with the opposite signs. For $N > 2$, the configuration matrix A for (13) always satisfies $\mathrm{Rank}(A) = N$ regardless of γ, which means that the configuration becomes a vortex crystal with $\dim \mathrm{Null}(A) = 1$. Then the strength $\Gamma_m(\gamma)$ of the mth point vortex and the speed V_0 belongs to the one-dimensional null-space spanned by the right eigenvector $\boldsymbol{v}_{N+1}(\gamma)$ to the zero singular value $\sigma_{N+1} = 0$. Owing to one-dimensional freedom, we choose the extended strength vector $\boldsymbol{\Gamma}(\gamma)$ by normalizing the right eigenvector $\boldsymbol{v}_{N+1}(\gamma)$ so that its L^2 norm up to N components becomes the unity, namely

$$\boldsymbol{\Gamma}(\gamma) = \frac{\boldsymbol{v}_{N+1}(\gamma)}{\sqrt{\sum_{k=1}^{N} \Gamma_k^2(\gamma)}}, \tag{14}$$

in which $\Gamma_m(\gamma)$ and $V_0(\gamma)$ are the mth component and the $N+1$ component of the normalized strength vector $\boldsymbol{\Gamma}(\gamma)$, respectively.

Figure 2 shows the strengths $\boldsymbol{\Gamma}(\gamma)$ of longitudinal N-rings for various N. First, we find that the identical point vortices cannot be a vortex crystal along the longitude, since $[1, 1, \ldots, 1, V_0]^T \notin \mathrm{Span}(\boldsymbol{\Gamma})$ for any V_0, which is in contrast with the latitudinal N-ring (12). Figure 2(a) indicates that, when the number of point vortices is odd, the strengths are positive for all γ satisfying the following periodicity owing to the discrete rotational symmetry.

$$\Gamma_1(\gamma_0) = \Gamma_2(0), \cdots, \Gamma_k(\gamma_0) = \Gamma_{k+1}(0), \cdots, \Gamma_N(\gamma_0) = \Gamma_1(0).$$

The point vortex with the strongest vortex strength is always located in the inner region of the torus where the curvature is negative, that is to say, the strongest one is $\Gamma_1(\gamma)$ for $\gamma \in [0, \gamma_0/2)$ and $\Gamma_N(\gamma)$ for $\gamma \in [\gamma_0/2, \gamma_0)$. For even cases, the situation is different from the odd cases as we see in Figure 2(b). The magnitude $|\Gamma_m(\gamma)|$ stays at the same level, while their signs are the opposite. To be specific, with $N = 2M$, we observe

$$\Gamma_1(\gamma) = \Gamma_3(\gamma) = \cdots = \Gamma_{2M-1} > 0, \qquad \Gamma_2(\gamma) = \Gamma_4(\gamma) = \cdots = \Gamma_{2M} < 0 \tag{15}$$

up to numerical tolerance.

The speed of the latitudinal rotation $V_0(\gamma)$, which is not shown here, is almost zero for even N, while it has a small variation with the magnitude of $O(10^{-4})$ for $N = 3$ but it vanishes as N increases. The entropy ratio $\omega_N(\gamma/\gamma_0)$ for $\gamma \in [0, \gamma_0)$ is plotted in Figure 3(a). It becomes less dependent on γ and its magnitudes decreases as odd N gets larger. This indicates that the point configuration of the longitudinal N-ring gets well-organized as N increases. We now change the aspect ratio α and observe the linear stability of the longitudinal N-ring. Panels (b) and (c) of Figure 3 show the log plots of the real part of the maximum eigenvalue $\mu_{\mathcal{L}}^N(\gamma)$ corresponding to the linearized matrix around the vortex crystal (13) for $\gamma \in [0, \gamma_0)$. The

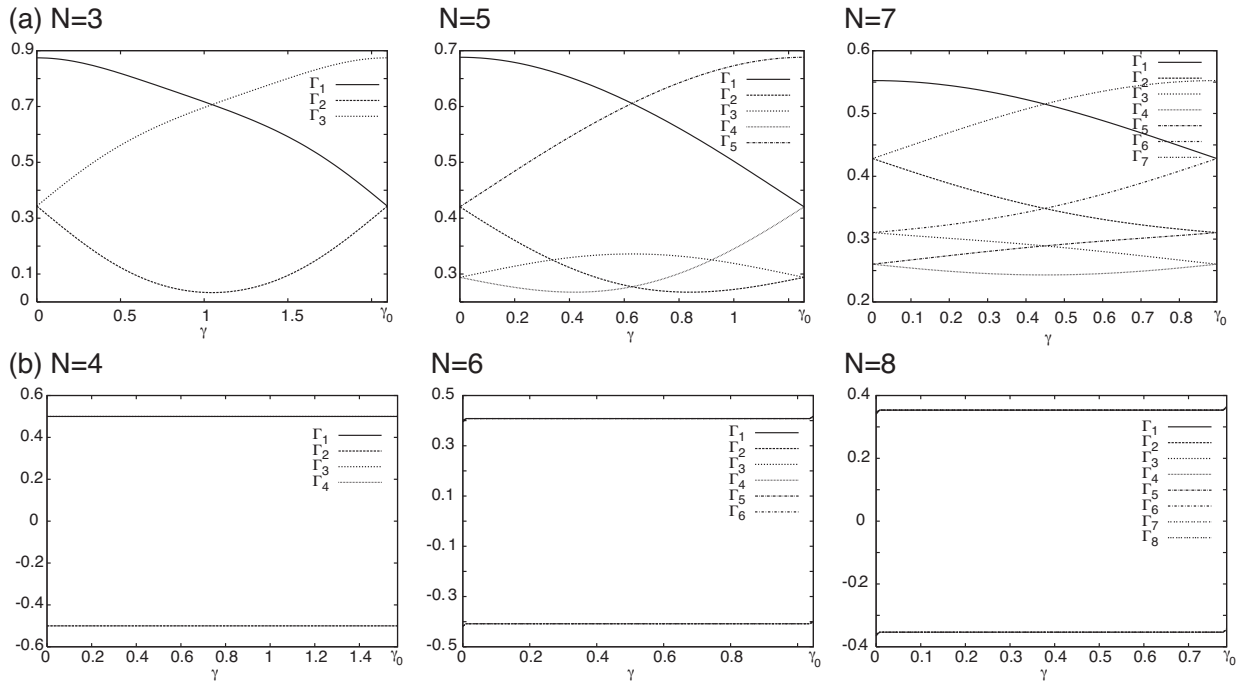

Figure 2: The strengths $\{\Gamma_m(\gamma)\}_{m=1}^N$ for $\gamma \in [0, 2\pi/N)$, when the number of point vortices is (a) $N = 3$, 5, 7 (odd) and (b) $N = 4$, 6, 8 (even).

strengths are chosen from the normalized extended strengths vector. The aspect ratio varies from $\alpha = 1.5$ to $\alpha = 10$. Since $\mu_{\mathcal{L}}^N(\gamma)$ are all positive, the vortex crystals are linearly unstable. For $N = 3$ in Figure 3(b), the vortex crystals for $\gamma \in [0, \gamma_0/2)$, where the number of point vortices in the inner region is larger than those in the outer region, are more unstable than those for $\gamma \in [\gamma_0/2, \gamma_1)$. For $N = 4$ in Figure 3(c), the profiles are almost flat and tend to a certain positive constant as α gets larger.

We increase the number of point vortices. As far as we have confirmed, longitudinal N-rings of $N \leqq 400$ are vortex crystals for any γ. Their corresponding configuration matrix A has a one-dimensional null-space. Since the speed V_0 is almost zero and γ_0 becomes smaller for large N, we focus on the vortex crystal of $\gamma = 0$ to observe how the distribution of the strengths converges as N increases. By normalizing the strengths so that $\Gamma_m = \Gamma(\theta_m)$ with $\theta_m = 2\pi m/N$, we regard them as a distribution $\Gamma(\theta)$ on $\theta \in [0, 2\pi)$, which is plotted in Figure 4. For odd N, the distribution $\Gamma(\theta)$ tends rapidly to a positive continuous function as $N \to \infty$ as in Figure 4(a). This indicates that the longitudinal N-ring configuration converges a longitudinal vortex sheet with the circulation distribution $\Gamma(\theta)$. The distribution has the maximum value at the innermost point of the negative curvature $\theta = 0$ and the minimum at the outermost point of the positive curvature $\theta = \pi$. On the other hand, the strength distribution for even N inherits the same sing-changing property as that of (15) and becomes oscillatory. As N goes to infinity, the arrangement of point vortices seems to converge a continuous "sheet" configuration, but the circulation distribution along the curve becomes a discontinuously sign-changing singular one, which is unphysical.

3.2 K-aligned/staggered M-rings

For positive integers K and M, we consider a configuration of point vortices, where K latitudinal M-rings are arranged evenly in the longitudinal direction. Its configuration is specified by

$$\vartheta_{k,m} = \frac{2\pi}{K}(k-1) + \gamma, \qquad \varphi_{k,m} = \frac{2\pi}{M}(m-1) + \Phi_k, \qquad k = 1, \ldots, K, \qquad m = 1, \ldots, M, \tag{16}$$

in which $\gamma \in [0, \gamma_1)$ with $\gamma_1 = 2\pi/K$ and $\Phi_k \in \mathbb{R}/2\pi\mathbb{Z}$ denote the longitudinal and latitudinal phase differences between M-rings respectively. For $\Phi_k = 0$, the configuration is called *a K-aligned M-ring*, while

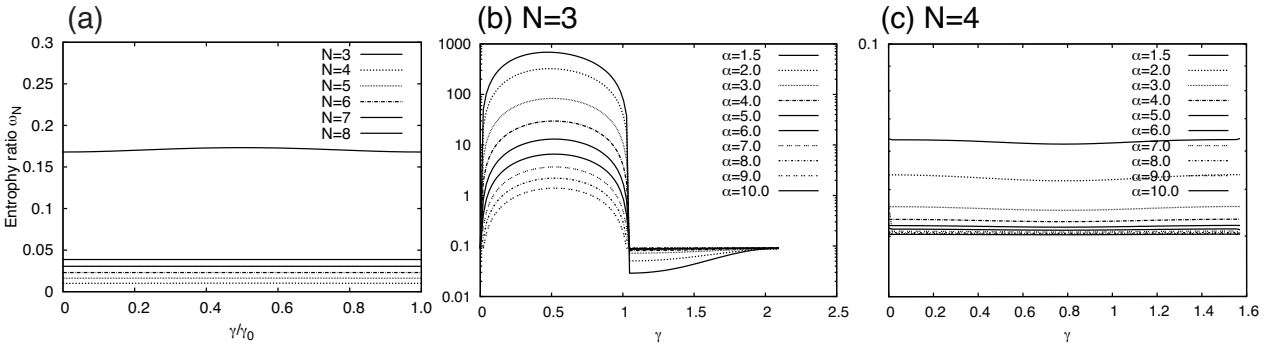

Figure 3: (a) Plots of the entropy ratio $\omega_N(\gamma/\gamma_0)$ for $N = 3, \ldots, 8$. (b,c) Log plots of the maximum of the real part of the eigenvalues $\mu_{\mathcal{L}}^N(\gamma)$ corresponding to the longitudinal N-rings for $N = 3$ and $N = 4$ respectively. The aspect ratio varies from $\alpha = 1.5$ to $\alpha = 10$.

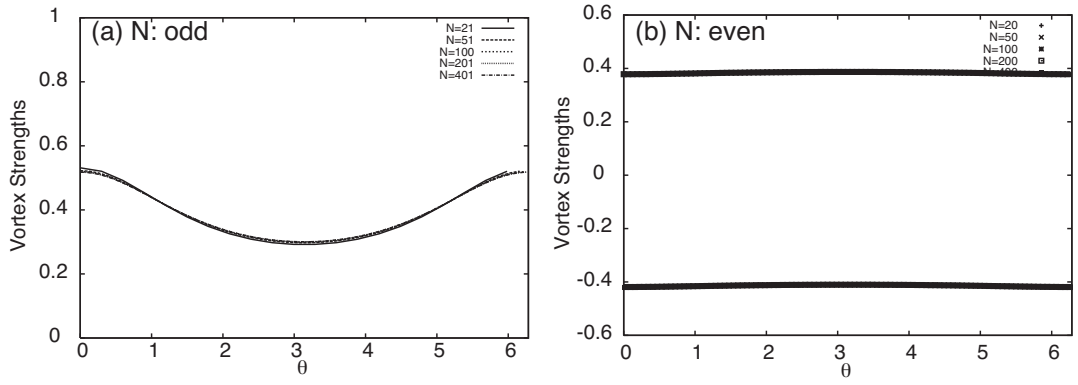

Figure 4: Distributions of the vortex strength $\Gamma(\theta)$ for $\theta \in [0, 2\pi)$ corresponding to longitudinal N-rings of (a) $N = 21$, 51, 101, 201, 401 (odd) and (b) $N = 20$, 50, 100, 200, 400 (even).

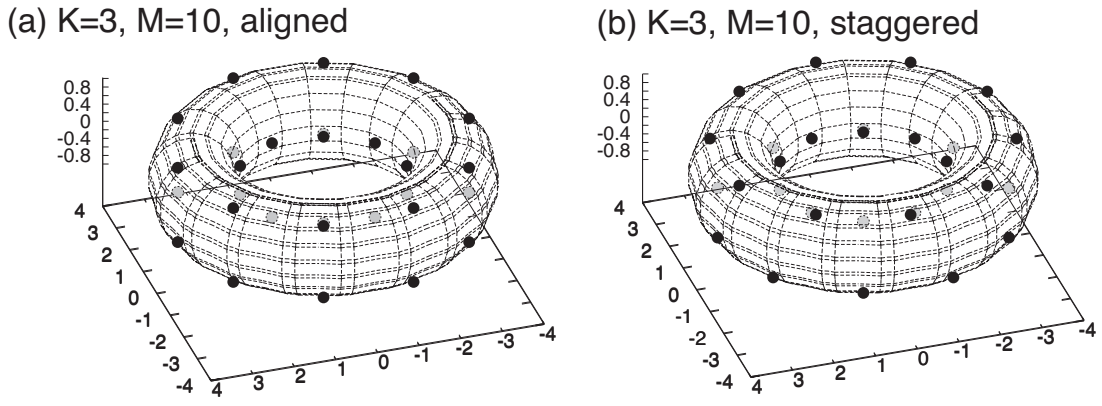

Figure 5: (a) The 3-aligned 10-ring and (b) the 3-staggered 10-ring for $\gamma = 0$ in (16).

it is referred to as *a K-staggered M-ring* when $\Phi_k = \frac{2\pi}{M}(k \mod 2)$. We note that $N = KM$ is the total number of point vortices of this configuration.

For $K = 1$, this configuration is nothing but a single M-ring (12), which is always a vortex crystal with the identical strength [32]. The 2-aligned/staggered M-ring is a special case of relative equilibria, called pairs of M-rings that has also been considered in [32]. Accordingly, in what follows, we focus on the case of $K \geqq 3$. Figure 5 shows the illustration of the 3-aligned/staggered 10-rings with $\gamma = 0$ in 3D Euclidean space. When we change γ, each of the latitudinal M-rings slides in the longitudinal direction. As far as we have examined, for any $\gamma \in [0, 2\pi/K)$ with $K = 3$ and any $3 \leqq M \leqq 10$, 3-aligned/staggered M-rings are always vortex crystals whose corresponding configuration matrices have a one-dimensional null-space. We thus normalize the right eigenvector to the zero eigenvalue in the same manner as (14) in §3.1 to obtain the strengths, which is denoted by $\Gamma_{k,m}(\gamma)$ for the mth point vortex on the kth M-ring. As a matter of fact, we find that M point vortices on the same line of latitude (M-ring) have the same strength. In other words, $\Gamma_{k,m}(\gamma)$ is independent of m. Hence, we consider the representative strength $\widetilde{\Gamma}_k(\gamma) \equiv \Gamma_{k,m}(\gamma)$ for the kth vortex ring in what follows.

Figure 6 is the plots of the representative strengths $\{\widetilde{\Gamma}_k(\gamma)\}_{k=1}^K$ for $\gamma \in [0, \gamma_1)$ with $\gamma_1 = 2\pi/K$. When $K = 3$, they are all positive, namely, $\widetilde{\Gamma}_k(\gamma) > 0$. In addition, owing to the discrete rotational symmetry in the longitudinal direction, we observe $\widetilde{\Gamma}_1(0) = \widetilde{\Gamma}_3(\gamma_1)$, $\widetilde{\Gamma}_2(0) = \widetilde{\Gamma}_1(\gamma_1)$, $\widetilde{\Gamma}_3(0) = \widetilde{\Gamma}_2(\gamma_1)$ for the aligned configuration, and $\widetilde{\Gamma}_1(0) = \widetilde{\Gamma}_3(\gamma_1)$, $\widetilde{\Gamma}_3(0) = \widetilde{\Gamma}_1(\gamma_1)$, $\widetilde{\Gamma}_2(0) = \widetilde{\Gamma}_2(\gamma_1)$ for the staggered configurations. We also notice that the strength $\widetilde{\Gamma}_2(\gamma)$ of the second vortex ring becomes the largest for all γ. In other words, the outermost vortex ring located in the positive curvature region has the maximum representative strength. When $K = 4$, the sign of the strengths changes alternately, i.e., $\widetilde{\Gamma}_1(\gamma)$, $\widetilde{\Gamma}_2(\gamma) > 0$ and $\widetilde{\Gamma}_3(\gamma)$, $\widetilde{\Gamma}_4(\gamma) < 0$. Owing to the discrete rotational symmetry, they satisfy $\widetilde{\Gamma}_1(0) = -\widetilde{\Gamma}_4(\gamma_1)$, $\widetilde{\Gamma}_2(0) = -\widetilde{\Gamma}_1(\gamma_1)$, $\widetilde{\Gamma}_3(0) = -\widetilde{\Gamma}_2(\gamma_1)$ and $\widetilde{\Gamma}_4(0) = -\widetilde{\Gamma}_3(\gamma_1)$ for both configurations. We find numerically that the K-aligned/staggered M-rings with $K = 3$, 4 and $M = 10$ become vortex crystals for the aspect ratios $\alpha = 1.5, \ldots, 10$. Regarding the linear stability, we confirm that $\mu_{\mathcal{L}}^N > 0$ for $\gamma \in [0, \gamma_1)$ and they are thus linearly unstable, although the plots of $\mu_{\mathcal{L}}^N$ are not shown here to avoid redundancy.

Fixing $M = 10$, we increase the number of latitudinal rings. For $K = 5$, 6, 7 and 8, the K-aligned/staggered 10-rings become vortex crystals whose configuration matrices have a one-dimensional null-spaces except for the case of $K = 6$ and 8 with $\gamma = 0$, in which the dimension of the null-space is two. Since the strengths of the point vortices on the same latitude are equivalent as observed for the cases of $K = 3$ and $K = 4$, we again observe on the normalized representative strengths $\{\widetilde{\Gamma}_k(\gamma)\}_{k=1}^K$ for $\gamma \in [0, \gamma_1)$ with $\gamma_1 = 2\pi/K$. Figure 7(a) and (b) show the plots of the representative strengths $\{\widetilde{\Gamma}_k(\gamma)\}_{k=1}^K$ of K-aligned/staggered 10-rings for odd $K = 5$ and 7 respectively. They are positive and satisfy the same periodicity as in $K = 3$. To be precise, we have

$$\widetilde{\Gamma}_1(0) = \widetilde{\Gamma}_K(\gamma_1), \quad \widetilde{\Gamma}_2(0) = \widetilde{\Gamma}_1(\gamma_1), \cdots, \widetilde{\Gamma}_k(0) = \widetilde{\Gamma}_{k-1}(\gamma_1), \cdots, \widetilde{\Gamma}_K(0) = \widetilde{\Gamma}_{K-1}(\gamma_1)$$

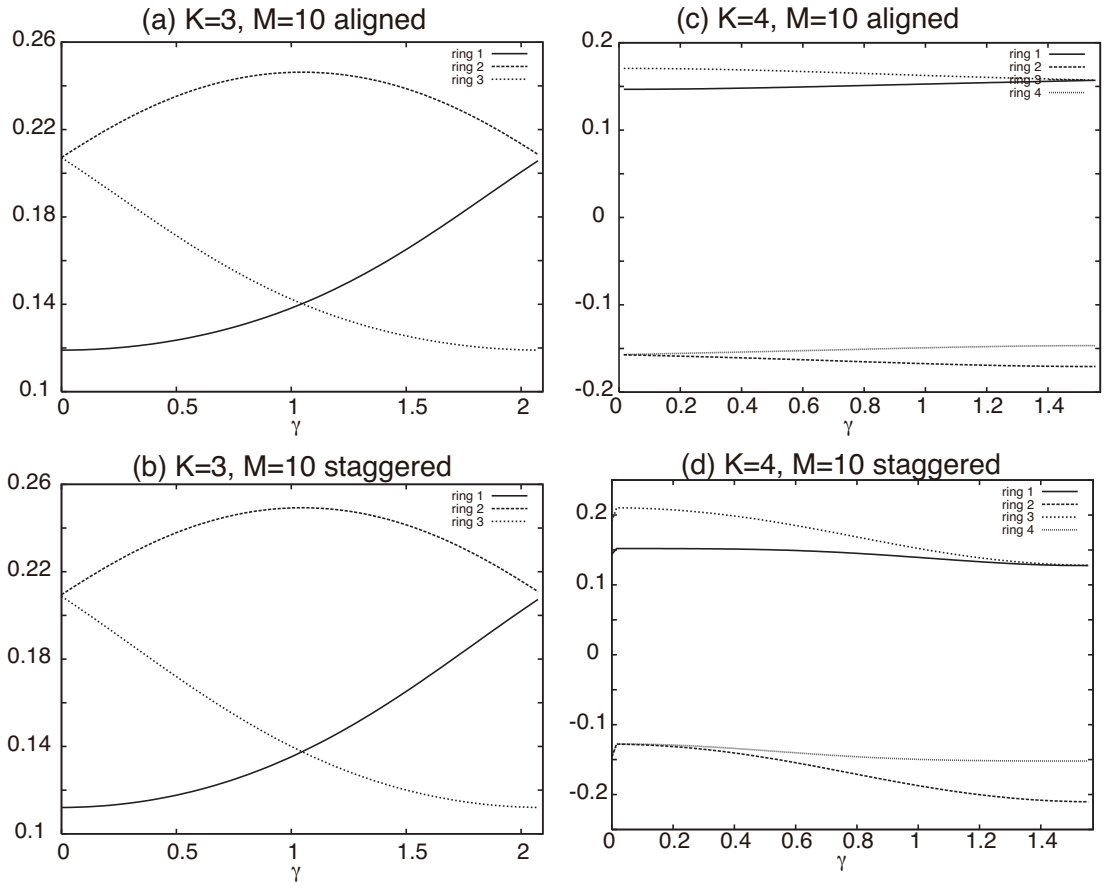

Figure 6: The representative strengths $\widetilde{\Gamma}_k(\gamma)$ of K latitudinal 10-rings for $\gamma \in [0, \gamma_1)$ with $\gamma_1 = 2\pi/K$. (a,b) Aligned and stasggered configurations for $K = 3$. (c,d) Aligned and staggered configurations for $K = 4$.

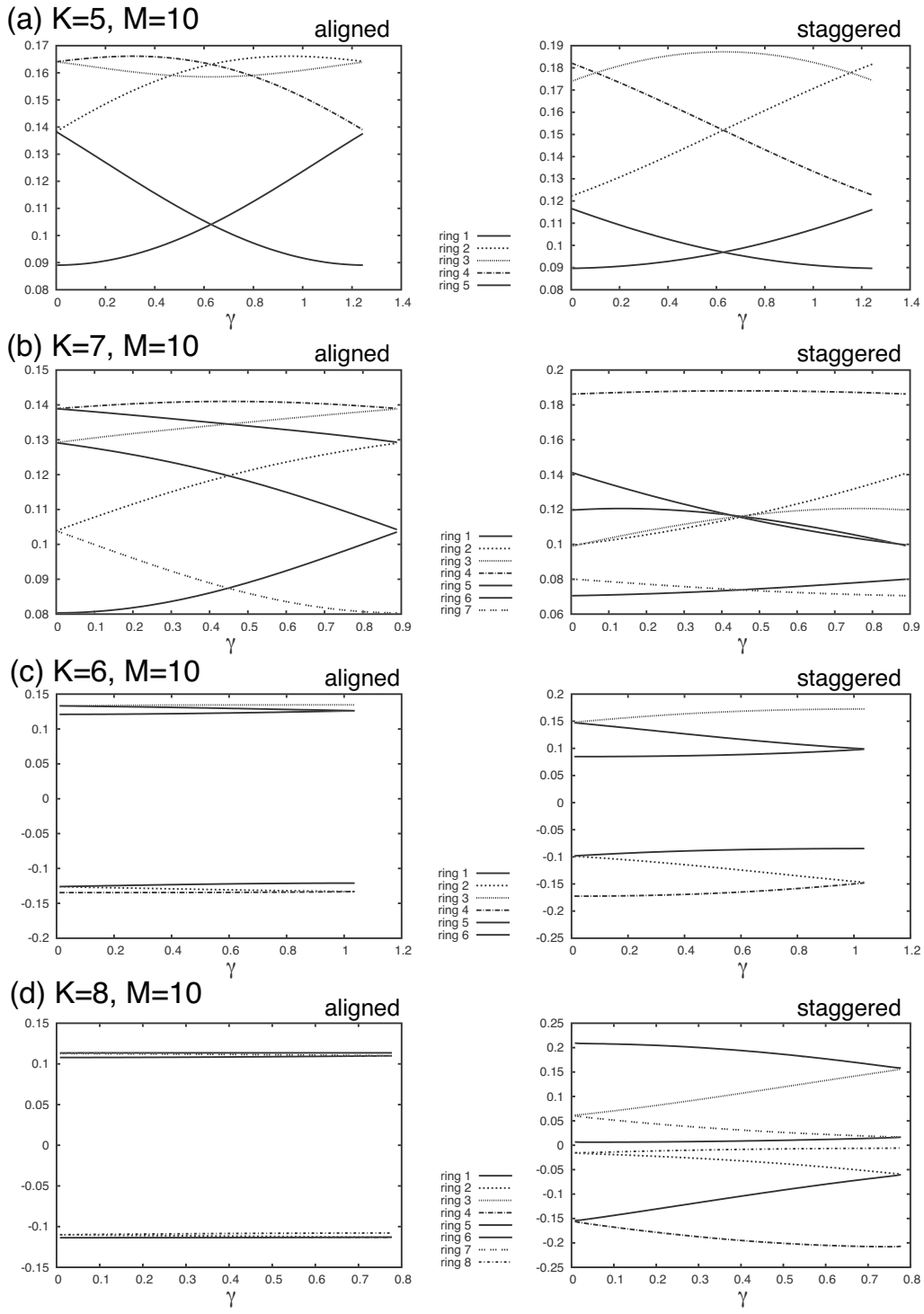

Figure 7: The representative strengths $\{\widetilde{\Gamma}_k(\gamma)\}_{k=1}^{K}$ of K-aligned/staggered 10-rings for (a) $K = 5$, (b) $K = 7$, (c) $K = 6$ and (d) $K = 8$.

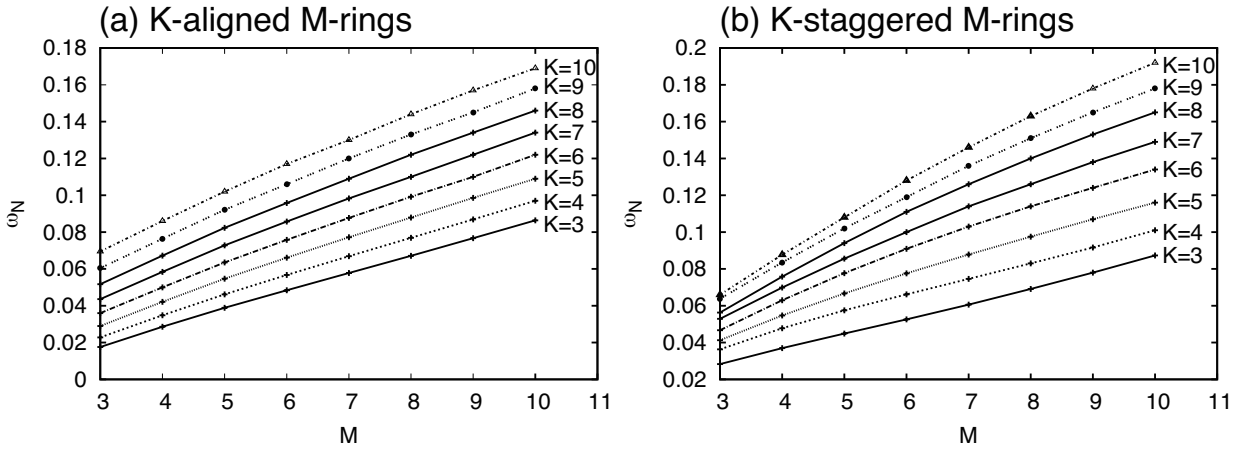

Figure 8: Entropy ratio ω_N for (a) K-aligned M-rings and (b) K-staggered M-rings. The aspect ratio of the torus is $\alpha = 3.0$.

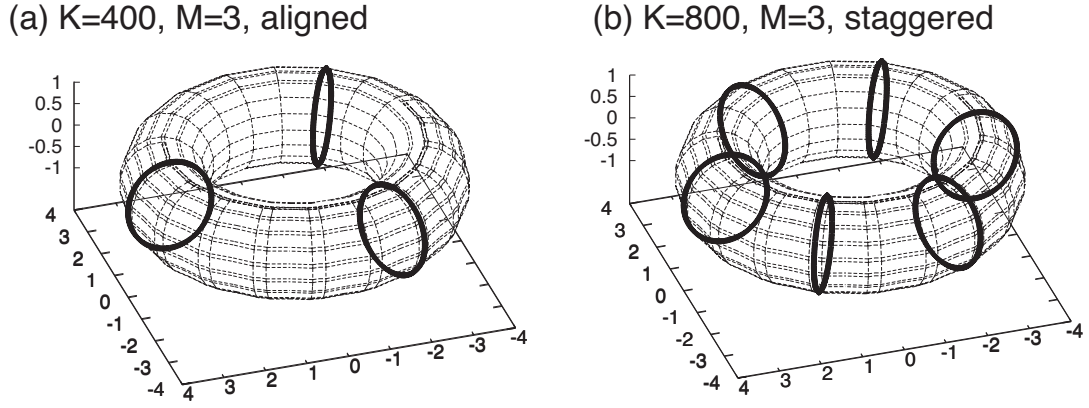

Figure 9: (a) The 400-aligned 3-rings and (b) the 800-staggered 3-rings on the toroidal surface of aspect ratio $\alpha = 3.0$ with $R = 3$ and $r = 1$ in 3D Euclidean space $\mathbb{E}^3$.

for aligned configurations and

$$\widetilde{\Gamma}_{\widetilde{K}}(0) = \widetilde{\Gamma}_{\widetilde{K}}(\gamma_1), \quad \widetilde{\Gamma}_k(0) = \widetilde{\Gamma}_{\widetilde{K}-k+1}(\gamma_1), \quad \widetilde{\Gamma}_{\widetilde{K}-k+1}(0) = \widetilde{\Gamma}_k(\gamma_1), \quad k = 1, \ldots, \widetilde{K}$$

for staggered configurations with $K = 2\widetilde{K}-1$. For even $K = 6$ and 8, as shown in Figure 7(c,d) respectively, the sign of the strength changes alternately and the discrete rotational symmetry gives rise to

$$\widetilde{\Gamma}_1(0) = -\widetilde{\Gamma}_K(\gamma_1), \quad \widetilde{\Gamma}_2(0) = -\widetilde{\Gamma}_1(\gamma_1), \cdots, \widetilde{\Gamma}_k(0) = -\widetilde{\Gamma}_{k-1}(\gamma_1), \cdots, \widetilde{\Gamma}_K(0) = -\widetilde{\Gamma}_{K-1}(\gamma_1),$$

which is consistent with the case of $K = 4$.

Figure 8 shows the entropy ratio ω_N of K-aligned/staggered M-rings with $\gamma = 0$ for $K = 3, \ldots, 10$ and $M = 3, \ldots, 10$. In both cases, the ratio increases monotonically as K and M get larger, which is equivalent to say that the distribution of point vortices over the toroidal surface tends to be uniform as $N = KM$ increases. On the other hand, comparing Figure 8(a) and (b), the staggered configurations have higher entropy ratio than the aligned ones, which is consistent with the fact that the points of the staggered configuration fills the toroidal surface in a more scattered manner than those of the aligned configurations.

We consider many latitudinal rings to see the limiting behavior of K-layered 3-rings for $K \leqq 800$. As far as we have confirmed numerically, those configurations are always vortex crystals with a one-dimensional null-space. Figure 9 shows the 400-aligned 3-rings and the 800-staggered 3-rings illustrated in 3D Euclidean space. As K gets larger, the aligned configuration tends to three longitudinal curves around the handle of the torus, while we have the convergence of six longitudinal curves for the staggered configuration. Generally, K-aligned/staggered M-rings tend to $M/2M$ longitudinal continuous curves as $K \to \infty$. Since point vortices on each of the longitudinal K-rings have the same strengths, we pay attention to the distribution of the representative strengths along one of the longitudinal curves around the handle. We define $\widetilde{\Gamma}(\theta_k) = \widetilde{\Gamma}_k(0)$ for $\theta_k = 2\pi/K$. When K is odd, for aligned configurations, the value of $\widetilde{\Gamma}(\theta_k)$ converges to a continuous distribution as shown in Figure 10(a). This is consistent with the distribution of a single longitudinal vortex sheet as shown in Figure 4. However, for staggered configurations, their value change discontinuously. Specifically, the strength of every three vortex rings forms a continuous curve and so we observe three curves in Figure 10(b). In the meantime, for even K, the distribution of the vortex strength of the aligned configurations for $K = 50$, 100, 200 and 400 in Figure 10(c) are almost identical two uniform lines with the opposite signs. For staggered configurations, the distribution converges very slowly to four distributions that are composed of the strengths of every four layers.

4 Vortex crystals on helical curves

In the previous section, vortex crystals are constructed based on the "ansatz-based" approach, in which we assume certain discrete rotational symmetries both in the longitudinal and latitudinal directions. Here, we explore the existence of another family of vortex crystals that are specific to the toroidal geometry: the existence of a handle structure. Let us notice that the fundamental group associated with the toroidal surface has two non-trivial generators, say, x and y, corresponding to loops rotating in the latitudinal and longitudinal directions respectively. Then any element in the fundamental group is expressed by $x^p y^q$ for p and $q \in \mathbb{Z}$, which is realized as a curve in 3D Euclidean space that is homotpic to the following helical curve $\boldsymbol{x}_h^{(p,q)}$ defined on $\mathbb{R}/2\pi\mathbb{Z}$:

$$\boldsymbol{x}_h^{(p,q)} : s \in \mathbb{R}/2\pi\mathbb{Z} \mapsto ((R - r\cos ps)\cos qs, (R - r\cos ps)\sin qs, r\sin ps) \in \mathbb{E}^3.$$

We will find vortex crystals that are arranged along the helical curve in what follows.

4.1 Asymmetric vortex crystals

The simplest choice of N points is an evenly spaced arrangement on the helical curve. Namely, setting $s_m = \frac{2\pi}{N} m$ for $m = 1, \ldots, N$, we simply check whether or not the configuration matrix corresponding to $(\vartheta_m, \varphi_m) = (ps_m, qs_m)$ has a zero singular value. However, unfortunately, this is not the case. Therefore, we need to look for a good configuration of N point vortices along the helical curve $\boldsymbol{x}_h^{(p,q)}$ in a random manner.

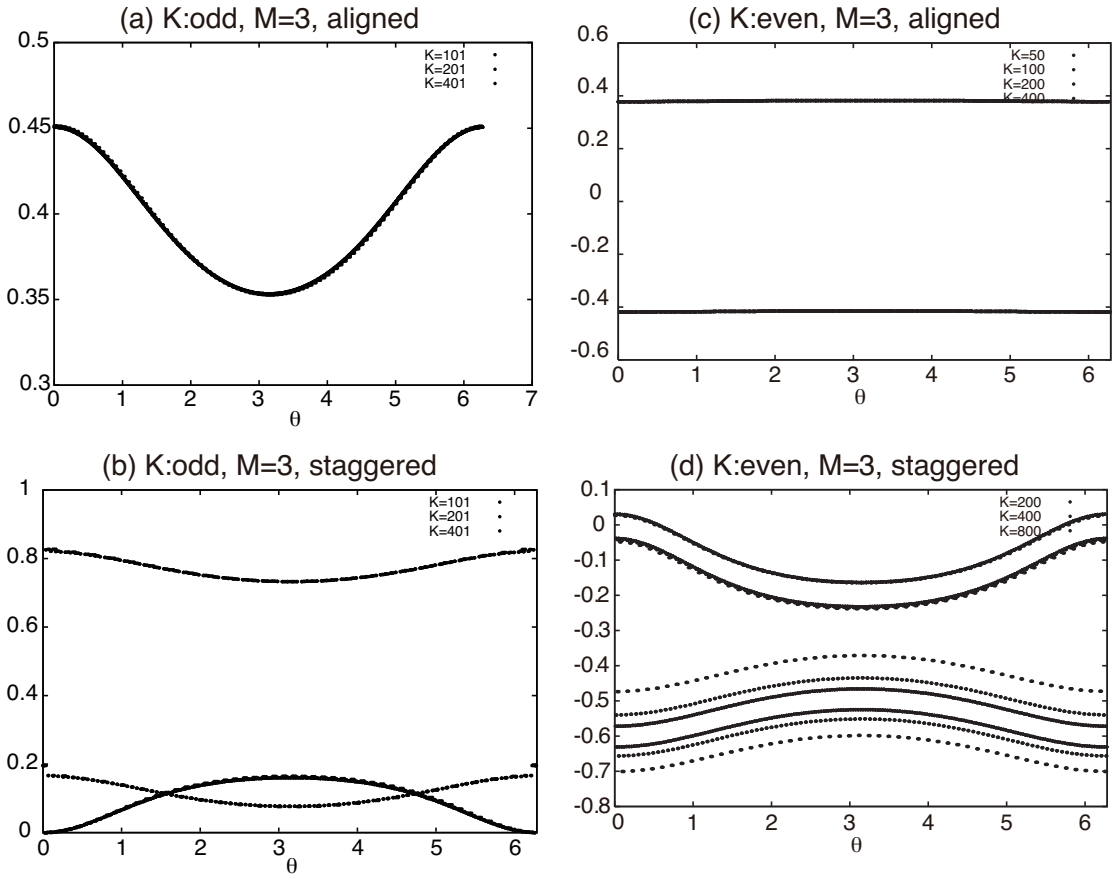

Figure 10: Distributions of the representative strengths and the singular values for (a) K-aligned 3-rings with $K = 101, 201, 401$, (b) K-staggered 3-rings with $K = 101, 201, 401$, (c) K-aligned 3-rings with $K = 50, 100, 200, 400$ and (d) K-staggered 3-rings with $K = 200, 400, 800$.

To accomplish this task, we use the Brownian ratchet scheme developed by Newton and Chamoun [28]. Without loss of generality, we assume that p and q are coprime positive integers so that the map $\boldsymbol{x}_h^{(p,q)}$ becomes injective. For given (p,q) and N, letting N points move randomly along the curve, we find vortex crystals as follows.

(i) [Guess the initial location] For $m = 1, \ldots, N$, sampling ξ_m from the uniform distribution on $[0, \frac{2\pi}{N})$, we set $s_m = \frac{2\pi}{N} m + \xi_m$. For each trial, we compute the singular values of the configuration matrix for $(\vartheta_m, \varphi_m) = (ps_m, qs_m)$. Repeating this step many times, we store the locations $\{s_m\}_{m=1}^N$ where the minimum singular value becomes the smallest. The initial guess of the ratchet scheme is given by this configuration with the smallest singular value, say, $\sigma_{\min}$, among the trials. This step is done only once.

(ii) [Ratchet scheme] For $m = 1, \ldots, N$, taking samples $\widetilde{\xi}_m$ from the normal Gaussian distribution of mean 0 and variance $\sigma_{\min}$ and setting $\widetilde{s}_m = s_m + \widetilde{\xi}_m$, we compute the smallest singular value $\widetilde{\sigma}_{\min}$ of the configuration matrix for $\{\widetilde{s}_m\}_{m=1}^N$. If $\widetilde{\sigma}_{\min} \leq \sigma_{\min}$, we renew the locations, i.e., $s_m = \widetilde{s}_m$ for $m = 1, \ldots, N$, and set $\sigma_{\min} = \widetilde{\sigma}_{\min}$, otherwise the trial is discarded.

(iii) [Terminate the ratchet] The process is repeated until $\widetilde{\sigma}_{\min}$ falls below a certain predetermined threshold, which is set to be of $O(10^{-13})$ in this paper. We call the final state as an approximated configuration of a vortex crystal.

(iv) [Post processing] The strengths $\{\Gamma_m\}_{m=1}^N$ of point vortices and the latitudinal speed V_0 are found from the basis set consisting of the extended strength vector for the null space. Since all vortex crystals shown here has one-dimensional null space, i.e., $\mathrm{Rank}(A) = N$, normalizing the right singular vector $\widetilde{\boldsymbol{\Gamma}}$ to the zero singular value so that $\sum_{m=1}^N \Gamma_m^2 = 1$, we obtain the strengths and the latitudinal speed.

The ratchet scheme successfully generates vortex crystals for $3 \leqq N \leqq 8$ on the helical curves $\boldsymbol{x}_h^{(p,q)}$ with $p+q = 3, 4, 5$. On the other hand, for $N \geqq 9$, the algorithm hardly converges, indicating that the singular value $\widetilde{\sigma}_{\min}$ falls into a non-zero local minimum with a positive value. This is a drawback of the ratchet algorithm originating from its stochastic nature, since the dimension of the search space for the random walk gets larger. This phenomenon was observed in the studies of vortex crystals on the sphere [29, 30].

Figure 11 shows vortex crystals of eight point vortices on the helical curves $\boldsymbol{x}_h^{(p,q)}$ with $p = 3, 4, 5$ on the toroidal surface of aspect ratio $\alpha = 3.0$ in 3D Euclidean space. They are asymmetric point vortex equilibria and their corresponding normalized strengths $\{\Gamma_m\}_{m=1}^8$ are listed in Table 4.1. Catalogues of vortex crystals of N point vortices from $N = 3$ to $N = 7$ are shown in Figure 12 for $p+q = 3$ and 4, and in Figure 13 for $p+q = 5$. They are illustrated as point configurations in the annulus $\{\zeta \in \mathbb{C} \,|\, \rho < |\zeta| < 1\}$ in the complex ζ-plane defined through the stereographic projection (1). In each panel, the helical curve $\boldsymbol{x}_h^{(p,q)}$ corresponding to the element $x^p y^q$ of the fundamental group is drawn as dashed curves. The strengths of the point vortices corresponding to the vortex crystals of Figure 12 and 13 are listed in Table 2 and Table 3 respectively. The vortex crystals in Figures 11, 12 and 13 are linearly unstable except for the case of $N = 5$ and $(p,q) = (1,2)$.

4.2 Helical longitudinal rings

As we observed in the previous section, when the number of the randomly moving points gets larger, it is more difficult to obtain vortex crystals on the helical curves. This is due to the increase of the search-space dimension for the random walk in the Brownian ratchet scheme. To deal with this difficulty, by imposing a certain constraint on point configurations and exploring a smaller dimensional search space, we obtain vortex crystals consisting of many point vortices. Let (p,q) be a given pair of coprime positive integers. Suppose now that we choose L lines of latitudes, $\phi_\ell \in \mathbb{R}/2\pi\mathbb{Z}$ for $\ell = 1, \ldots, L$, going around the handle of the toroidal surface. Then, each longitudinal line intersects with the helical curve $\boldsymbol{x}_h^{(p,q)}$ at q points. We thus generate $N = Lq$ point configurations aligned along the helical curve. In other words, the point

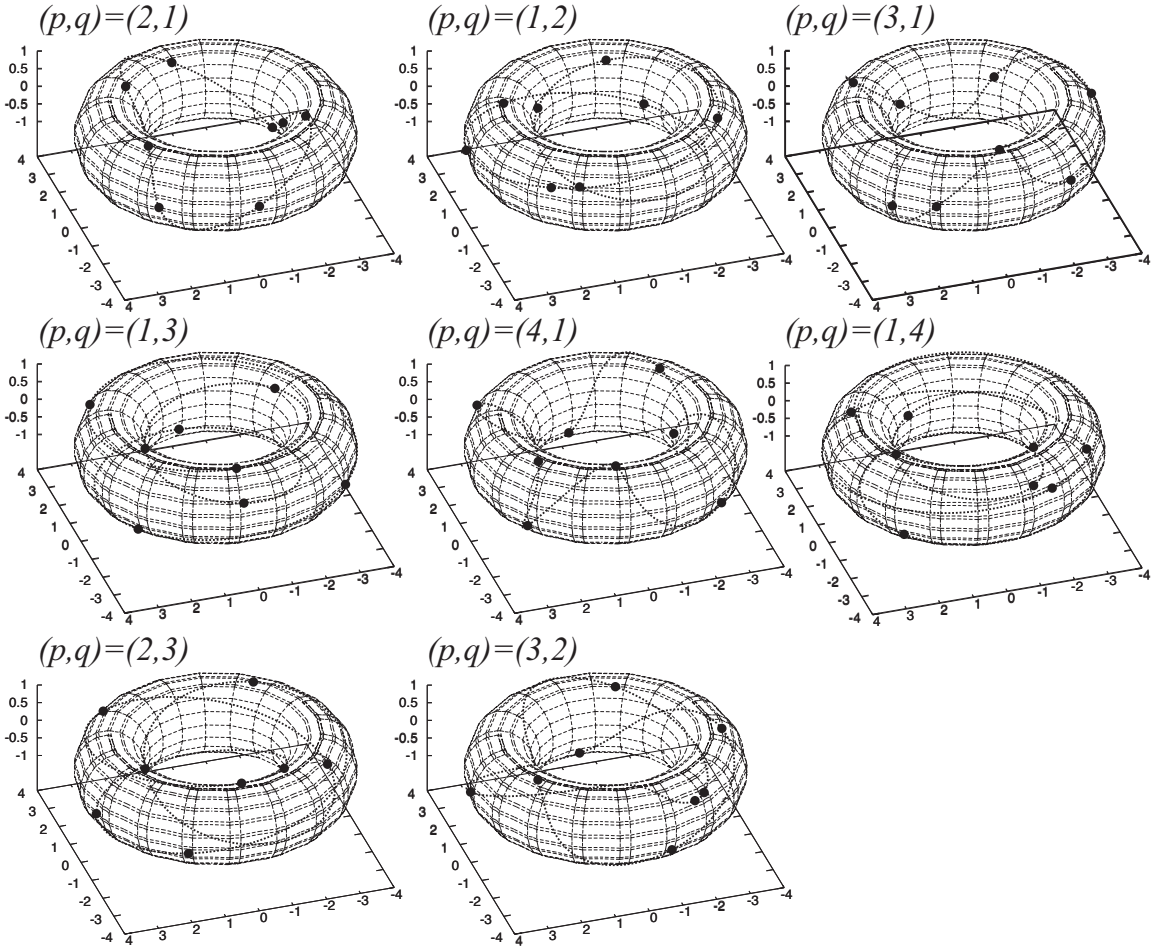

Figure 11: Vortex crystals consisting of eight point vortices along the helical curves $\boldsymbol{x}_h^{(p,q)}$ on the toroidal surface of aspect ratio $\alpha = 3.0$ for the pairs of coprime positive integers (p, q) with $p + q = 3$, 4 and 5. The dashed curves represent the helical curves. They are all linearly unstable.

(p, q)	Γ_1	Γ_2	Γ_3	Γ_4	Γ_5	Γ_6	Γ_7	Γ_8
$(2, 1)$	2.924e-2	4.666e-1	2.524e-1	4.666e-1	2.924e-2	4.666e-1	2.524e-1	4.666e-1
$(1, 2)$	2.592e-1	4.140e-1	2.950e-1	-4.047e-1	1.021e-1	-2.120e-1	-3.613e-2	6.738e-1
$(3, 1)$	5.154e-1	-2.428e-1	4.529e-1	-1.669e-1	3.302e-1	-1.844e-1	4.732e-1	-2.746e-1
$(1, 3)$	1.144e-1	4.254e-1	1.208e-1	2.155e-1	4.865e-1	4.993e-1	5.019e-1	8.379e-2
$(4, 1)$	1.613e-1	3.835e-1	3.347e-1	4.010e-1	3.903e-1	4.021e-1	3.146e-1	3.755e-1
$(1, 4)$	1.076e-1	-4.445e-2	5.141e-1	-4.837e-2	-5.262e-1	-1.519e-1	-6.474e-1	-2.859e-2
(3.2)	7.966e-1	2.127e-1	9.448e-3	-2.626e-4	-5.353e-1	-1.290e-2,	8.214e-2	1.629e-1
$(2, 3)$	2.105e-2	3.393e-1	6.571e-1	5.421e-2	4.608e-1	-1.263e-1	4.596e-1	1.005e-1

Table 1: Normalized strengths $\boldsymbol{\Gamma} = (\Gamma_1, \cdots, \Gamma_8)$ of eight point vortices on the helical curves $\boldsymbol{x}_h^{(p,q)}$ with the pairs of coprime positive integers (p, q) corresponding to Figure 11.

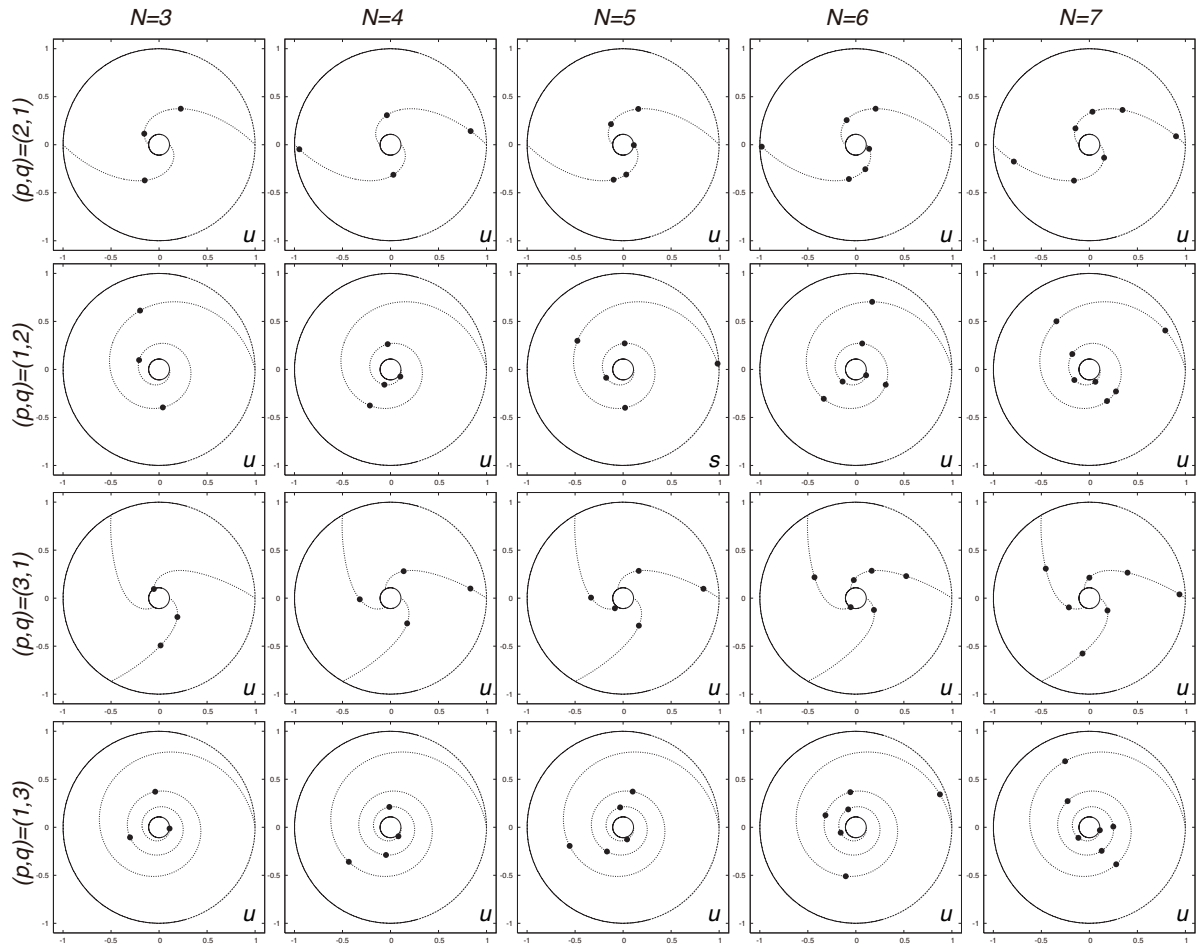

Figure 12: Vortex crystals consisting of $N = 3-7$ point vortices on the helical curves $\boldsymbol{x}_h^{(p,q)}$ for $(p, q) = (2, 1)$, $(1, 2)$, $(3, 1)$ and $(1, 3)$. In each panel, the points are illustrated as filled circles in the annular domain $\{\zeta \in \mathbb{C} \,|\, \rho < |\zeta| < 1\}$ that are mapped by the stereographic projection (1) and the helical curve is drawn as dashed curves. Symbols "u" and "s" indicate that the point vortex configuration is linearly unstable and neutrally stable respectively.

(p,q)	N	Γ_1	Γ_2	Γ_3	Γ_4	Γ_5	Γ_6	Γ_7
$(2,1)$	3	6.260e-1	7.690e-2	7.760e-1				
	4	3.262e-1	5.980e-1	3.109e-1	6.628e-1			
	5	7.472e-1	-2.884e-1	5.681e-1	1.631e-1	-9.621e-2		
	6	3.916e-3	5.163e-1	-2.366e-1	7.591e-1	-1.345e-1	2.885e-1	
	'7	1.112e-1	4.066e-1	6.026e-2	5.329e-1	3.175e-1	3.732e-1	5.428e-1
$(1,2)$	3	5.026e-1	8.583e-1	-1.033e-1				
	4	1.369e-1	6.994e-1	-2.095e-1	-6.695e-1			
	5	6.711e-1	3.864e-1	4.093e-1	3.238e-1	3.576e-1		
	6	3.658e-2	-4.457e-1	5.478e-1	-4.106e-2	4.384e-1	-5.532e-1	
	7	6.098e-1	4.128e-1	-3.213e-3	8.849e-4	1.577e-1	4.690e-1	4.614e-1
$(3,1)$	3	2.102e-1	9.716e-1	1.091e-1				
	4	1.457e-1	4.613e-1	7.180e-1	5.005-1			
	5	4.855e-2	-5.598e-1	-5.351e-1	3.237e-2	-6.300e-1		
	6	2.919e-1	1.404e-1	2.919e-1	4.714e-1	6.046e-1	4.714e-1	
	7	4.616e-2	3.478e-1	4.265e-1	3.624e-1	4.236e-1	3.907e-1	4.812e-1
$(1,3)$	3	7.052e-1	2.315e-1	6.701e-1				
	4	6.777e-1	5.856e-1	-4.091e-1	1.743e-1			
	5	6.620e-1	5.878e-1	1.833e-1	-4.264e-1	-2.795e-2		
	6	7.877e-1	4.996e-1	2.311e-2	2.780e-1	1.642e-1	1.585e-1	
	7	1.836e-1	-4.000e-1	-3.502e-1	2.061e-1	2.826e-1	-4.269e-1	-6.157e-1

Table 2: Normalized strengths $\mathbf{\Gamma} = (\Gamma_1, \cdots, \Gamma_N)$ of N point vortices corresponding to Figure 12.

(p,q)	N	Γ_1	Γ_2	Γ_3	Γ_4	Γ_5	Γ_6	Γ_7
$(4,1)$	3	5.784e-1	8.155e-1	-1.828e-2				
	4	5.000e-1	5.000e-1	5.000e-1	5.000e-1			
	5	4.481e-1	2.829e-1	4.264e-1	5.259e-1	5.108e-1		
	6	3.460e-1	3.754e-1	5.256e-1	3.979e-1	5.472e-1	7.311e-2	
	7	3.149e-1	1.890e-1	4.253e-1	3.747e-1	4.668e-1	3.571e-1	4.454e-1
$(1,4)$	3	1.699e-1	3.280e-1	9.294e-1				
	4	5.821e-1	-3.937e-1	2.821e-1	6.532e-1			
	5	7.340e-1	4.180e-1	-2.404e-1	3.489e-1	3.272e-1		
	6	4.555e-2	2.295e-1	3.528e-1	8.256e-1	2.308e-1	2.931e-1	
	7	6.083e-1	2.201e-2	1.553e-1	-5.972e-1	-1.018e-2	2.899e-1	4.056e-1
$(3,2)$	3	6.990e-1	-7.135e-1	-4.807e-2				
	4	5.563e-2	9.608e-1	2.690e-1	3.757e-2			
	5	4.929e-1	5.835e-1	5.717e-1	1.963e-1	-2.260e-1		
	6	2.716e-1	5.218e-1	-3.569e-2	1.930e-1	-5.648e-2	7.824e-1	
	7	5.151e-1	4.773e-1	4.297e-1	8.684e-3	-1.641e-1	4.454e-1	-3.112e-1
$(2,3)$	3	7.175e-1	4.055e-2	6.954e-1				
	4	4.910e-1	-6.281e-1	-5.397e-1	2.700e-1			
	5	3.880e-1	5.895e-1	3.907e-1	5.197e-1	2.814e-1		
	6	1.260e-1	9.793e-1	9.145e-2	-3.739e-2	8.628e-2	8.835e-2	
	7	4.813e-1	1.645e-1	1.842e-1	1.384e-1	1.748e-1	8.048e-1	9.996e-2

Table 3: Normalized strengths $\mathbf{\Gamma} = (\Gamma_1, \cdots, \Gamma_N)$ of N point vortices corresponding to Figure 13.

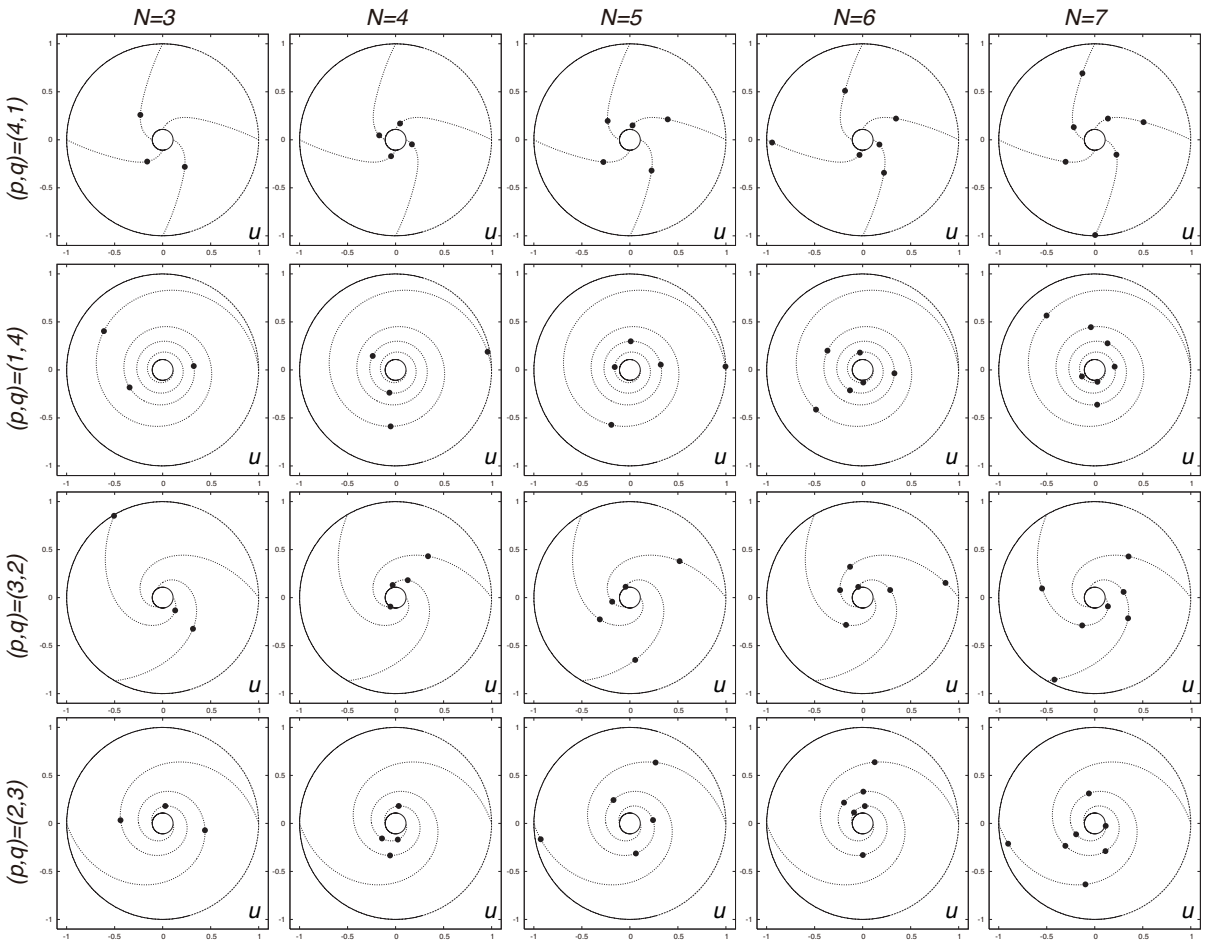

Figure 13: Vortex crystals consisting of $N = 3-7$ point vortices on the helical curves $\boldsymbol{x}_h^{(p,q)}$ for $(p, q) = (4, 1)$, $(1, 4)$, $(3, 2)$ and $(2, 3)$. In each panel, the points are illustrated as filled circles in the annular domain $\{\zeta \in \mathbb{C} \,|\, \rho < |\zeta| < 1\}$ that are mapped by the stereographic projection (1) and the helical curve is drawn as dashed curves. Symbols "u" and "s" indicate that the point vortex configuration is linearly unstable and neutrally stable respectively.

configuration forms L longitudinal q-rings revolving helically around the handle. We investigate whether the point configuration can be a vortex crystal for an appropriate choice of $\{\phi_\ell\}_{\ell=1}^L$.

For instance, taking naively $\phi_\ell = \frac{2\pi}{L}(\ell-1)$ for $\ell = 1,\dots,L$, we set the $N = Lq$ parameters as $s_{\ell,m} = \frac{\phi_\ell}{q} + \frac{2\pi}{q}(m-1) \in \mathbb{R}/2\pi\mathbb{Z}$ for $m = 1,\dots,q$ so that the points at $(\vartheta_{\ell,m}, \varphi_{\ell,m}) = (ps_{\ell,m}, qs_{\ell,m})$ are on the helical curve $\boldsymbol{x}_h^{(p,q)}$. Then we find that the smallest singular value of the configuration matrix corresponding to this point configuration is not zero. Accordingly, allowing the L latitudinal lines move randomly, we search for L longitudinal q-rings along the helical curve $\boldsymbol{x}_h^{(p,q)}$ that form vortex crystals using the following modified Brownian ratchets scheme:

(i) [Guess the initial location] For $\ell = 1,\dots,L$, sampling ξ_ℓ from the uniform distribution on $[-\frac{\pi}{L}, \frac{\pi}{L})$, we set $\phi_\ell = \frac{2\pi}{L}(\ell - 0.5) + \xi_\ell$. For each trial, we obtain $s_{\ell.m} = \frac{\phi_\ell}{q} + \frac{2\pi}{q}(m-1)$ for $\ell = 1,\dots,L$ and $m = 1,\dots,q$, from which we compute the singular values of the configuration matrix for $(\vartheta_{\ell,m}, \varphi_{\ell,m}) = (ps_{\ell,m}, qs_{\ell,m})$. Repeating this step many times, we store the locations $\{\phi_\ell\}_{\ell=1}^L$ where the minimum singular value becomes the smallest. The initial guess of the ratchets scheme is given by the configuration having the smallest singular value, say, $\sigma_{\min}$, among the trials. This step is done only once.

(ii) [Ratchet scheme] For $\ell = 1,\dots,L$, taking samples $\widetilde{\xi}_\ell$ from the normal Gaussian distribution of mean 0 and variance $\sigma_{\min}$ and setting $\widetilde{\phi}_\ell = \phi_\ell + \widetilde{\xi}_\ell$, we compute the smallest singular value $\widetilde{\sigma}_{\min}$ for the configuration matrix corresponding to $\{\widetilde{\phi}_\ell\}_{\ell=1}^L$. If $\widetilde{\sigma}_{\min} \le \sigma_{\min}$, we renew the locations, $\phi_\ell = \widetilde{\phi}_\ell$ for $\ell = 1,\dots,L$, and set $\sigma_{\min} = \widetilde{\sigma}_{\min}$, otherwise the trial is discarded.

(iii) [Terminate the ratchet] The process is repeated until $\widetilde{\sigma}_{\min}$ falls below the threshold of $O(10^{-13})$.

(iv) [Post processing] When the dimension of the null space of the configuration matrix is one, the strengths Γ_m and the latitudinal speed V_0 are obtained as the basis set consisting of the extended strength vector for the null space. Normalizing the right singular vector to the zero singular value so that $\sum_{m=1}^N \Gamma_m^2 = 1$, we obtain the strengths and the velocity.

For $L = 1$, it is nothing but a single longitudinal q-ring, which is always a vortex crystal as shown in § 3.1. When $L = 2$, the modified Brownian ratchet scheme provides vortex crystals for any $q = 2,\dots,19$ and $p < q$. That is to say, for each pair of (p,q), there exists a real $\gamma_2^{(p,q)} \in [0,\pi)$ such that the two q-rings are aligned along the longitudinal lines at $\phi_1 = \gamma_2^{(p,q)}$ and $\phi_2 = \gamma_2^{(p,q)} + \pi$, which are the two sections of the toroidal surface cut by the plane $-x\sin\gamma_2^{(p,q)} + y\cos\gamma_2^{(p,q)} = 0$ in 3D Euclidean space. For $L \geqq 3$, the ratchet scheme hardly converges, except that we obtain vortex crystals when $L = 3, 5, 7$ and $q = 5, 3, 7, 11, 13, 17, 19$ are prime numbers, and p are multiples of L less than q. Then the longitudinal lines $\{\phi_\ell\}_{\ell=1}^L$ are evenly spaced in the latitudinal direction. To be specific, for each (p,q), there exists a real $\gamma_L^{(p,q)}$ such that the longitudinal q-rings are arranged helically on the lines of latitude $\phi_\ell = \frac{2\pi}{L}(l-1) + \gamma_L^{(p,q)}$ for $l = 1,\dots,L$. This observation gives rise to the following conjecture.

Conjecture 1. *Let L and q be prime numbers, and $p < q$ be multiples of L. Then there exists a real $\gamma_L^{(p,q)} \in [0, 2\pi/L)$ such that L longitudinal q-rings consisting of the intersection points between the helical curve $\boldsymbol{x}_h^{(p,q)}$ and the lines of latitude $\phi_\ell = \frac{2\pi}{L}(l-1) + \gamma_L^{(p,q)}$ form a vortex crystal.*

These vortex crystals are referred to as L *helical longitudinal q-rings* on the curve $\boldsymbol{x}_h^{(p,q)}$. As examples, we show the vortex crystals for $L = 7$ and $q = 19$ consisting of $N = Lq = 133 = 19\cdot 7$ point vortices arranged helically along the curve $\boldsymbol{x}_h^{(p,q)}$ for $p = 7$ and $p = 14$ in Figure 14(a) and (b) respectively. In both panels, the seven longitudinal 19-rings are evenly spaced in the latitudinal direction, revolving around the handle in the longitudinal direction along the helical curve. Since those 19-rings on the latitudinal line have the same strength distribution, we thus plot the strengths of point vortices on one of the longitudinal 19-rings for $(p,q) = (7,19)$ and $(14,19)$ in Figure 14(c) and (d) respectively, which indicate that the strengths are positive and the distribution depends on the number of branches p.

Let us summarize the properties of the L helical longitudinal q-rings for $L = 3$, 5, 7 and $q = 5$, 7, 11, 13, 17, 19. The strengths of the point vortices are positive and all longitudinal q-ring have the same

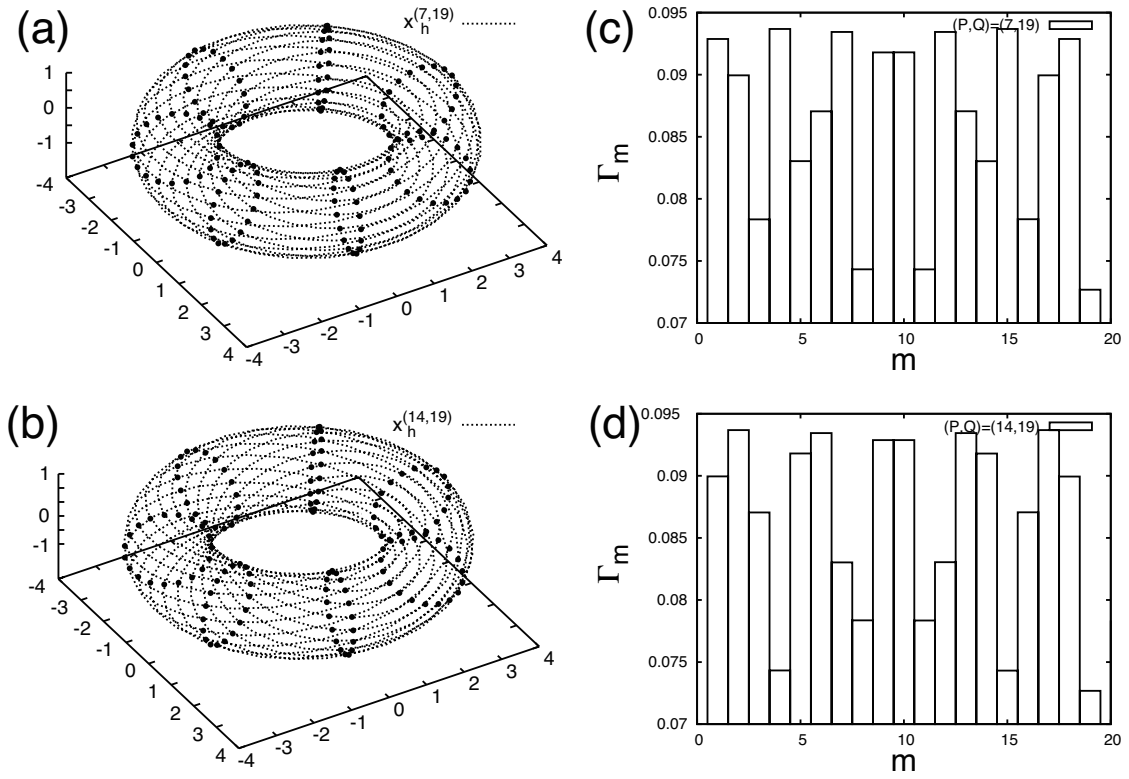

Figure 14: Point configurations of $L = 7$ helical longitudinal 19-rings for (a) $p = 7$ and (b) $p = 14$. They are vortex crystals consisting of $N = 133 = 19 \cdot 7$ points arranged helically along the curves $\boldsymbol{x}_h^{(7,19)}$ and $\boldsymbol{x}_h^{(14,19)}$, which are drawn as dotted curves, respectively. Their normalized strengths $\Gamma_1, \ldots, \Gamma_{19}$ corresponding to one of the longitudinal rings on the same longitude are plotted for (c) $(p, q) = (7, 19)$ and (d) $(p, q) = (14, 19)$.

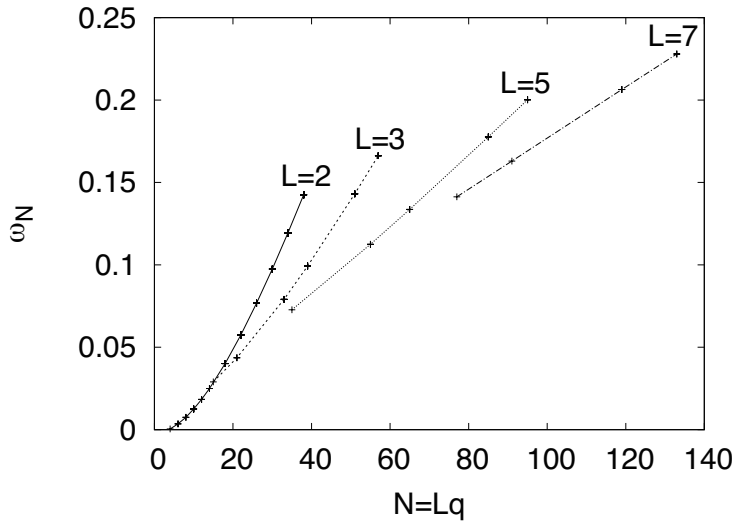

Figure 15: Entropy ratio ω_N for L helical longitudinal q-rings on the curve $\boldsymbol{x}_h^{(p,q)}$ for $L = 2, 3, 5, 7$ and $q = 5, 7, 11, 13, 17, 19$. The number of point vortices is $N = Lq$.

strength distribution. This is consistent with what we have observed in § 3.2 for K-aligned/staggered M-rings with odd M, since $N = Lq$ is odd. They are all linearly unstable since we confirm numerically $\mu_{\mathcal{L}}^N > 0$ for those configurations. The entropy ratios for those vortex crystals with respect to $N = Lq$ are plotted in Figure 15, which shows that the ration increases as N gets larger. Comparing the entropy ratio with those for K-aligned/staggered M-rings in Figure 8(a) and (b), we find that helical longitudinal q-rings tend to acquire a larger entropy ratio for the same N. This means that the point vortices on the twisted longitudinal q-rings spread in a complicated manner on the surface of the torus than K-aligned/staggered M-rings.

5 Concluding remarks

5.1 Vortex crystals and the toroidal geometry

We obtain vortex crystals on the surface of a torus, in which relative configuration of point vortices are unchanged with rotating in the latitudinal direction at a constant speed. Regarding the equations (7) and (8) as a linear null equation for the configuration matrix, we look for point configurations whose corresponding configuration matrix becomes rank-deficient. The strengths of point vortices and the latitudinal speed of rotation belong to the null space of the configuration matrix. All calculations are performed via the singular value decomposition of the configuration matrix, which is much easier than solving the equations as a nonlinear equation with respect to point locations for given strengths.

To find rank-deficient configuration matrices, we have adopted an ansatz-based approach and/or a stochastic approach. The ansatz-based approach reveals that longitudinal N-rings and K-aligned/staggered M-rings become vortex crystals. Those vortex crystals are linearly unstable regardless of the aspect ratio of the torus, which is in contrast with latitudinal N-ring configurations whose linear stability depends on the aspect ratio [33]. When the number of point vortices on the latitudinal ring is odd, the strengths of point vortices are positive and their distribution varies in accordance with the curvature of the torus. As we increase the number of point vortices, each longitudinal vortex ring converges to a longitudinal vortex sheet with a continuous positive strength distribution. On the other hand, when the number of point vortices is even, the sign of the strengths change alternately. As a result, each vortex ring tends to an unphysical "vortex sheet" with a singular sign-changing distribution as the number of point vortices gets larger.

We have also found vortex crystals of N point vortices on the curve $\boldsymbol{x}_h^{(p,q)}$ winding around the handle

of the torus for a pair of coprime integers p and q with $p < q$. They are obtained by allowing N points random walk on the curve using the Brownian ratchet scheme. For small N, the Brownian ratchet scheme generates asymmetric vortex crystals, which are linearly unstable. In addition, combining an ansatz-based approach with the ratchet scheme, we obtain vortex crystals, called L helical longitudinal q-rings, consisting of $N = Lq$ points located at the intersection points between L equi-spaced longitudinal lines and the curve $\boldsymbol{x}_h^{(p,q)}$ for primes L and q, and $p(< q)$ that are multiples of L. Those helical vortex crystals are all linearly unstable.

To summarize, vortex crystals obtained in this paper give rise to longitudinal point configurations that are specific to the existence of the handle structure of the torus. Let us remember that the Brownian ratchet scheme has been utilized to obtain many vortex crystals in the plane [28] and on the surface of a sphere [29]. Comparing the present results with the preceding ones, the ratchet scheme is less probable to find vortex crystals on the toroidal surface. We expect that it substantially stems from the inhomogeneity of the toroidal geometry that is less symmetric than the plane and the spherical surface with a constant curvature. It is interesting to consider the number of vortex crystals for given N on the toroidal surface in comparison with those on the spherical surface.

In connection with the configurations of quantized vortices, the longitudinal N-ring for odd N is not realizable, since the ration of their strengths cannot be integers generically as we see in Figure 2(a). On the other hand, the longitudinal N-ring for even N may be always realizable, while the magnitudes of the vortex strength are almost the same. The other vortex crystals obtained in the paper fail to have quantized strengths. This may be remedied by adding a special flow called "pore" flow on the surface of a torus as discussed in [10, 25], which will be a future study.

5.2 Vortex crystals and point configurations on manifolds

The problem of finding vortex crystals is closely related to finding "good" point configurations on manifolds that are used quadrature rules, computer design and interpolation of functions in the finite element scheme. Apart from the particle-interaction based approach adopted in this paper, one can take another approach to find good point configurations that minimize a given energy function. The most famous problem is finding a set of N points $\omega_N = \{x_i\}_{i=1}^N$ over d'-dimensional compact set A embedded in d-dimensional Euclidean space that minimize the following Riesz s-energy $E_s(\omega_N)$.

$$\mathcal{E}_s(A, N) := \inf_{\omega_N \subset A} \sum_{i \neq j} |x_i - x_j|^{-s},$$

where $s > 0$ and $|\cdot|$ denotes Euclidean distance. The parameter s controls the particle interaction. If $s = 1$, the energy $E_1(\omega_N)$ is Coulomb energy corresponding to the classical potential theory of charged particles. As $s \to \infty$ with keeping N unchanged, this is equivalent to the best packing problem, while it becomes the minimizing problem of the following inter-particle energy with the logarithmic kernel,

$$\mathcal{E}_0(A, N) = \inf_{\omega_N \subset A} \sum_{i \neq j} \log |x_i - x_j|,$$

which has the same singularity of the Hamiltonian (9). See the review of this minimizing problems by Hardin and Saff [21]. One of the central issues of this problem is clarifying the behavior of $\mathcal{E}_s(A, N)$ as $N \to \infty$. See the results in [6, 7, 22] for d-rectifiable compact manifolds with Hausdorff dimension d_H, where $\mathcal{E}_s(A, N) = O(N^2)$ for $0 < s < d_H$ and $\mathcal{E}_s(A, N) = O(N^2 \log N)$ for $s \geqq d_H$. Another minimizing energy problem in connection with the quadrature rule on compact manifolds has been investigated by Damelin et al. [12, 13].

Let us finally discuss the relation between the minimizing point configurations and vortex crystals on compact surfaces. The spherical surface has been the main object, since the problems of $s = \infty$ and $s = 0$ are related to famous Tammes problem [35] and Smale's seventh problem [34]. See also the introduction and the reference list in Newton and Sakajo [29] in terms of the applications to many physical and biological problems, in which they discussed the connections between their point configurations and the optimal packings of the spherical surface. On the contrary, there are less results on point configurations on the toroidal surface. In the numerical simulation of finding point configurations minimizing Riesz s-energy

by Hardin and Saff [21], most of the points are distributed in the outer domain of the torus where the curvature is positive for small $s \ll 1$, while they spread uniformly for larger $s > 1$. Vortex crystals given here spread in the longitudinal and latitudinal directions evenly and their randomness has been measured through the entropy ratio associated with the configuration matrix. Although the Hamiltonian energy (9) has the same logarithmic singularity as $E_0(\omega_N)$, the ring configuration of point vortices in Sections 3 and 4 scatter over the surface and can not be a minimizer of the Hamilton energy, since the it is not positive definite, i.e., the Hessian around the configuration have the positive eigenvalues. The relation between the enery-minimizing point configurations and vortex crystals will also be an interesting future topic.

References

[1] J. R. Abo-Shaeer, C. Raman, J. M. Vogels and W. Ketterle. 2001 *Observation of vortex lattices in Bose-Einstein Condensates*, Science **292** pp. 476–479.

[2] A. A. Abrikosov. 1955 *On the magnetic properties os superconductors of the second group*, Soviet. Phys. J. Exp. Theoret. Phys. **32** pp. 1442–1452.

[3] A. A. Abrikosov. 2003 *Nobel lecture: Type-II superconductors and the vortex lattice*, Rev. Mod. Phys. **76** pp. 975–979.

[4] H. Aref and D. L. Vainchtein. 1998 *Point vortices exhibit asymmetric equilibria*, Nature **392** pp. 769–770. (doi:10.1038/33827)

[5] H. Aref, P. K. Newton, M. A. Stremler, T. Tokieda and D. L. Vainchtein. 2003 *Vortex crystals*, Adv. in Appl. Mech. **39**, pp. 1–79.

[6] S. V. Borodachov, D. P. Hardin and E. B. Saff. 2007 *Asymptotics for discrete weighed minimal Riesz energy problems on rectifiable sets*, Trans. Amer. Math. Soc. **360** No. 3 pp. 1559–1580.

[7] S. V. Borodachov, D. P. Hardin and E. B. Saff. 2007 it Asymptotics of best-packing on rectifiable sets, Proc. Amer. Math. Soc. **135** No. 8 pp. 2369–2380.

[8] H. E. Cabral, K. R. Meyer and D. S. Schmidt. 2003 *Stability and bifurcations for the $N+1$ vortex problem on the sphere*, Regular Chaotic Dyn. **8** pp. 259–282. (doi:10.1070/RD2003v008n03 ABEH000243)

[9] L. J. Campbell and R. Ziff. 1978 *A Catalog of Two-Dimensional Vortex Patterns*, LA-7384-MS, Rev., Informal report, Los Alamos Scientific Laboratory.

[10] A. Corrada-Emmanuel. 1994 *Exact solution for superfluid film vortices on a torus*, Phy. Rev. Lett. **72** pp. 681–684. (doi:10.1103/PhysRevLett.72.681)

[11] P. Chouraquit and G. Elber. 1996 *Physically based adaptive triangulation of freeform surfaces*, in Computer Graphics International 1996 (CGI ' 96), IEEE Computer Society Press, pp. 144–153.

[12] S. B. Damelin, J. Levesley, D. L. Ragozin and X. Sun. 2009 *Energies, group-invariant kernels and numerical integration on compact manifolds*, J. Complexity **25** pp. 152–162.

[13] S. B. Damelin, F. J. Hickernell, D. L. Ragozin and X. Zeng. 2010 *On energy, discrepancy and group invariant measures on measurable subsets of Euclidean space*, J Fourier Anal. Appl. **16** pp. 813–839. (doi: 10.1007/s00041-010-9153-2)

[14] P. Engels, I. Coddington, P. C. Haljan and E. A. Cornell. 2002 *Nonequilibrium effects of anisotropic compression applied to vortex lattices in Bose-Einstein Condensate*, Phys. Rev. Lett. **89** No.10 100403 (doi:10.1103/PhysRevLett.89.100403)

[15] P. Engels, I. Coddington, P. C. Haljan, V. Schweikhard and E. A. Cornell. 2003 *Observation of long-lived vortex aggregates in rapidly rotating Bose-Einstein condensates*, Phys. Rev. Lett. **90** No. 17 170405. (doi: 10.1103/PhysRevLett.90.170405)

[16] U. Essmann and H. Träuble. 1967 *The direct observation of individual flux lines in type II superconductors*, Phys. Rev. Lett. **1967** pp. 526–527.

[17] R. P. Feynmann. 1955 *Application of Quantum Mechanics to Liquid Helium*, Prog. Low Temp. Phys., edited by D. F. Brewer (North-Holland, Amsterdam) **1**, Chap. II. pp. 17–53.

[18] K. S. Fine, A. C. Cass, W. G. Flynn and C. F. Driscoll. 1995 *Relaxation of 2D turbulence and vortex crystal*, Phys. Rev. Lett. **75** No. 18 pp. 3277–3282.

[19] B. A. Grzybowski, H. A. Stone, G. M. Whitesides. 2000 *Dynamic self-assembly of magnetized, millimetre-sized objects rotating at a liquid-air interface*, Nature **405** pp. 1033–1036.

[20] D. Z. Jin and D. H. E. Dubin. 2000 *Characteristics of two-dimensional turbulence that self-organizes into vortex crystals*, Phys. Rev. Lett. **84** No. 7 pp. 1443–1446.

[21] R. H. Hardin and E. B. Saff. 2004 *Discretizing manifolds via minimum energy points*, Notices Amer. Math. Soc. **51** pp. 1186–1194.

[22] D. P. Hardin and E. B. Saff. 2005 *Minimal Riesz energy point configurations for rectifiable d-dimensional manifolds*, Adv. Math. **193** pp. 174–204.

[23] F. Laurent-Polz. 2002 *Point vortices on the sphere: a case of opposite vorticities*, Nonlinearity **15** pp. 143–171. (doi:10.1088/0951-7715/15/1/307)

[24] C. C. Lim, J. Montaldi and M. R. Roberts. 2001 *Relative equilibria of point vortices on the sphere*, Physica D **148** pp. 97–135. (doi:10.1016/S0167-2789(00)00167-6)

[25] J. Machta and R. A. Guyer. 1988 *Superfluid films in porous media*, Phys. Rev. Lett. **60** No.20 pp. 2054–2057.

[26] P. K. Newton. 2001 *The N-Vortex Problem, Analytic Techniques*, Appl. Math. Sci. **145** Springer Verlag, New York.

[27] P. K. Newton and G. Chamoun. 2009 *Vortex lattice theory: a particle interaction perspective*, SIAM Review **51** No. 3 pp. 501–542.

[28] P. K. Newton and G. Chamoun. 2007 *Construction of point vortex equilibria via Brownian ratchets*, Proc. R. Soc. A **463** pp. 1525–1540. (doi:10.1098/rspa.2007.1832)

[29] P. K. Newton and T. Sakajo. 2009 *Point vortex equilibria on the sphere via Brownian ratchets*, Proc. Roy. Soc. A **465** pp. 437–455. (doi:10.1098/rspa.2008.0203)

[30] P. K. Newton and T. Sakajo. 2010 *Point vortex equilibria and optimal packings of circles on sphere*, Proc. Roy. Soc. A **467** pp. 1468–1490. (doi:10.1098/rspa.2010.0368)

[31] T. Sakajo. 2012 *Fixed equilibria of point vortices in symmetric multiply connected domains*, Phys. D **241** pp. 583–599. (doi:doi:10.1016/j.physd.2011.11.021)

[32] T. Sakajo and Y. Shimizu. 2016 *Point vortex interactions on a toroidal surface*, Proc. Roy. Soc. A, vol. 472 20160271 (doi:10.1098/rspa.2016.0271)

[33] T. Sakajo and Y. Shimizu. 2018 *Toroidal geometry stabilizing a latitudinal ring of N point vortices on a torus*, J. Nonlinear Science. (doi: 10.1007/s00332-017-9440-z)

[34] S. Smale. 2000 *Mathematical problems for the next century*, in Mathematics: Frontiers and Perspectives, V. Arnold, M. Aliyah, P. Lax, and B. Mazur, eds., AMS, Providence, RI, pp. 271–294.

[35] P. M. L. Tammes. 1930 *On the origin of number and arrangements of the places of exit on the surface of pollen-grains*, Recl. Trav. Bot. Neerl. **27** pp. 1–84.

[36] W. Thomson. 1867 *On vortex atoms*, Phil. Mag. **34** pp. 15–24.

[37] A. M. Turner, V. Vitelli and D. R. Nelson. 2010 *Vortices on curved surfaces*, Rev. Mod. Phys. **82** pp. 1301–1348. (doi:10.1103/RevModPhys.82.1301)

[38] E. J. Yarmchuk and M. J. V. Gordon. 1979 *Observation of stationary vortex arrays in rotating superfluid helium*, Phys. Rev. Lett. **1979** pp. 214–217.

[39] A. P. Witkin and P. S. Heckbert 1994 *Using particles to sample and control implicit surfaces*, Computer Graphics, Proc. SIGGRPAH '94.